Masters Theses

Graduate College

6-2003

Effect of Modified Clay-Zeolite Pigment on the Viscoelastic, Optical, And Printing Properties of a LWC Gravure Coating

Lokendra Pal
Western Michigan University

Follow this and additional works at: https://scholarworks.wmich.edu/masters_theses

Part of the Materials Science and Engineering Commons

EFFECT OF MODIFIED CLAY-ZEOLITE PIGMENT ON THE VISCOELASTIC,
OPTICAL, AND PRINTING PROPERTIES OF A LWC GRAVURE COATING

by

Lokendra Pal

A Thesis
Submitted to the
Faculty of The Graduate College
in partial fulfillment of the
requirements for the
Degree of Master of Science
Department of Paper and Printing Science and Engineering

Western Michigan University
Kalamazoo, Michigan
June 2003

ACKNOWLEDGMENTS

EFFECT OF MODIFIED CLAY- ZEOLITE PIGMENT ON THE VISCOELASTIC, OPTICAL, AND PRINTING PROPERTIES OF A LWC GRAVURE COATING

Lokendra Pal, M.S.

Western Michigan University, 2003

This study investigates the influence of modified clay- zeolite pigment on the viscoelastic, optical, and printing properties of a LWC coating. Currently, lightweight, coated papers have experienced problems with mottle, distortion, fiber puffing and poor print quality when printed with water-based inks. However, water-based inks represent a proven solution to reducing volatile organic compound (VOCs) emissions. Poor wetting and ink spreading on the paper surface constitute the majority of print quality issues associated with the water-based printing of LWC papers.

Similar problems are encountered during the printing of ink jet papers due to high percentage of water contained in these inks. For this reason, porous pigments such as zeolites and high surface area silicas are used for these print applications. Zeolites, hydrated aluminosilicates, are microporous, high internal –surface area crystalline materials with a sponge like structure. The high void volume of these pigments is also known to improve the opacity of the coating layer, by increasing the number of air voids available to scatter light.

Comparison of a zeolite containing coating to a commercial formulation showed the zeolite to improve the optical and surface properties of the paper with no adverse effect on print quality.

TABLE OF CONTENTS

LIST OF TABLES

LIST OF FIGURES

CHAPTER I

INTRODUCTION

In the surface treatment of paper with aqueous systems or in the printing of paper by offset, or water-based flexography and rotogravure, water-paper interactions, although of short duration, may lead to undesirable changes in its structure. One of the most important effects is a roughening of the surface that impairs the print quality- this effect is particularly noticeable with wood containing papers. It has been suggested that processes causing roughening include stress relaxation, swelling and debonding (1, 2, 3).

As for the future of printing processes, ecology will play a much larger role, with special attention being paid to eliminating waste and emissions and reducing energy input. One main focal point will be the reduction of the volatile organic compounds (VOCs) released into the atmosphere. Water-based inks represent a proven solution to reducing volatile organic compound emissions. Water-based inks do not require the capital investment into explosion proof motors or solvent recovery systems and decrease atmospheric pollution; have less solvents, lower fire risks, less print odor; and are easier to wash-up on the press.

The main components of water-based inks are pigment, binding agent, carrier (water) and additives. The binding agent and additives are what mainly determine the ink properties. Binding agents are typically acrylic resins, which are emulsions or diluted to water with amines. The most common approach to developing resins for water-based gravure printing inks involves reacting a polymer bearing carboxylic acid groups with some type of alkali or amines. The resulting resin contains neutral salt groups, which are highly water-soluble. However, when the amines are evaporated, the resin reverts to its initial form and yields an insoluble ink with good resistance to moisture. The amines

1

must be chosen to evaporate on the printed surface and not in the cylinder cell (4). The proportion of these types of binding agents used is made to fit the printing process and the quality requirements of the final product. Additives used in water-based inks are antifoam, waxes, extenders, pH-controllers and surfactants. Surfactants work also as drying controllers. A typical water-based ink formulation may contain 20% pigment, 15% binding agents, 5% additives, and 60% water (7). The surface tensions of the water-based inks can range from 30-40 dyne/cm.

The print quality of publication gravure is controlled, in essence, by the physico-chemical interactions between paper and printing ink. Spreading of the wet ink, as well as setting and drying are most directly impacted by these interactions. In the case of solvent-based inks, the interactions are purely physical in nature. With water-based inks, however, the situation is much more complex. Water itself interacts with all the components of paper including pigments, binders and cellulose fibers causing paper sheet distortion (surface and bulk), but there are also chemical effects resulting, most notably, in pH changes within aqueous phase (5). Careful control of ink pH is required, when printed with water-based inks. Most water systems have a pH of over 9.0 (6).

Surface energy of water (approx. 72 dyne/cm) is substantially higher than that of most organic solvents, including toluene (26 dyne/cm), hence water has less tendency to wet low surface energy surfaces. Although the boiling point of water is lower than that of toluene, the amount of energy required to vaporize an equal amount of water is far higher (4) because of the high heat of vaporization due to hydrogen bond. Part of the water absorbs in the substrate and evaporates with time. As the water and amines evaporate, the diluted resins precipitate and the emulsion particles form a close packed hexagonal cell system. While coated boards are able to absorb water and reduce the need for drying, lightweight coated papers have less of a capacity to absorb the water, which causes running and quality problems. Similar problems are encountered during ink jet printing.

Coatings for ink jet printing are formulated with porous silicas to control the depth of penetration and feathering or bleeding of the ink (8, 9, 10). The similarities between ink jet and water based LWC print quality issues may therefore be resolved by following similar coating formulation principles. The use of silica or zeolites may be used to reduce problems with mottle, fiber swelling (puffing), surface roughening, and wrinkles due to the high amount of water absorbency that occurs (11) in the printing of LWC papers with water-based inks which are more environmental friendly. Zeolites have already been shown to be effective for inkjet coatings (10).

Coating structure of paper can affects how the ink is transferred to the surface, how the ink lies on the surface, how well the ink dries and is absorbed by the surface, and how well the press operator can control the register of the finished product. Absorption of inks during printing is controlled by the structure of the pore space near the coating surface. The porous structure of coating depends on the coating color formulation; pigments used and their combinations, chemical additives, and the coating and drying processes (12). For lightweight coated grades, a porous coating structure helps achieve higher gloss and smoothness at lower coating weight (13).

The aim of this work is to improve the coating formulations for the printing with water-based inks. A Cylindrical Laboratory Coater was used to apply select pigmented coatings onto a standard commercial lightweight basesheet. A Cerutti gravure press was used to print the samples with a standard alkaline water-based gravure ink.

CHAPTER II

LITERATURE REVIEW

Surface roughening arises from various factors in the interaction between ink and paper. Lepoutre and Skowronski analyzed the relationship between ink penetration and surface roughening, and suggested that ink penetration into paper causes stress relaxation, swelling and debonding (1, 2, 3). It is postulated that the main interaction causing surface roughening is the penetration of ink through the coating into the base paper, while the ink has fluidity.

The ink film thickness of rotogravure is much higher than flexo, creating a higher demand on the ink drying speed. The slower evaporation rate and alkaline nature of water-based inks over the solvent based inks leads to an increased cellulose fiber swelling (puffing), and causes the paper to curl and pucker, which results in greater surface roughness. This roughness can cause incomplete ink spreading and coverage, resulting in poor print quality, related to missing or skipped dots also called speckle or snowflaking (14, 15). Increased drying requirements can lead to image distortion, especially with lower basis weight absorbent papers (15, 16). The drying speed is not only influenced by the content of toluene in the ink, but also the absorbency of the paper.

Mottle occurs due to the non-uniform receptivity of the ink into the paper and can be detected from variations in ink density values. Mottle occurs with all types of printing processes; however, it is the major setback for the lightweight coated rotogravure papers. Image distortion is also a problem. Image distortion is the result of the asymmetrical expansion of the paper as the fibers swell when contacted with water. This is also known as fiber puffing. Distortion causes printed text to become unreadable and images to become unclear. Fiber puffing can also cause a weakening of the coating layer. As the

coating weakens, it does not adhere as well to the paper, causing problems with distortion when printed. Due to mottle and distortion, the overall print quality of these grades is low.

The rotogravure printing process requires direct contact of the image cylinder with the substrate. Thus, the substrate's roughness strongly influences print quality. When using solvent-based inks in the gravure process, uniform spreading and a minimal amount of paper fiber swelling occur. The use of alkaline water-based inks increases cellulose fiber swelling. Cellulose fibers are highly hydrophilic and readily wetted and swollen with water. This swelling leads to poor print quality, such as missing or skipped dots (17, 18). When skipped dots are encountered in printing with solvent inks, an electrostatic assist is employed (19, 20). However, the success of this technique hinges on the low conductivity of solvent inks. The conductivity of water-based inks is several orders of magnitude higher and does not permit the establishment of an electrical field between the impression roller and the cylinder. Consequently, ESA is less effective with water-based inks (4). The degree of hydrophobicity and hydrophilicity (hydrophilic-lypophilic balance) that will provide the best wetting with the least amount of fiber swelling is important to identify. Wetting and spreading of water-based inks on coated paper surfaces are estimated by measurement and calculations of contact angle, surface tension, surface energy and interfacial tension. Water-based inks do not wet and print smoothly due to the high surface tension of the water component.

It is thought that porous zeolite pigment, when incorporated into the coating, will improve mottle, fiber puffing and distortion, and wrinkles, along with improving brightness, opacity, compressibility, and absorbency of the final product. Zeolite pigments are a soft to moderately hard, light density mineral, most commonly known for its use in water filtration systems. Zeolites are microporous, high internal –surface area, and crystalline materials with well-defined structure. Because of their unique porous

properties, zeolites can absorb and loose water without damage to their crystalline structure (21, 22). The ability to absorb water and then have it removed by heat while keeping the original structure intact makes porous zeolite pigment a good candidate for a water-based gravure coating. The water-based gravure process currently uses high temperature dryers, so mottle and wrinkles occur more often with this printing method. When incorporating porous zeolite pigment, the coating will allow cationic additives to be used. A cationic additive, when used in the gravure process, modifies rheology and improves print quality (23).

According to Lepoutre (1978), the rate of water absorbency of a substrate may influence the composition and the structure of a paper coating (24). Rapid dewatering is used when gravure printing on LWC paper grades. Rapid dewatering is due to the openness of the coating structure, which causes a lower print quality due to mottle and wrinkling. It is thought that the porous zeolite pigment will reduce these problems by holding the water in the coating layer, thus preventing it from reaching the base sheet layer, which will reduce the mottle and wrinkling problems.

Delaminated clay and calcinated clay are the two most commonly used pigments in a LWC gravure coating; these pigments do not produce a sheet with high brightness or high opacity. Titanium dioxide is added to the formulation to help improve the appearance and smoothness of the coating sheet. Synthetic plastic pigments are also now being used to improve the smoothness and appearance. The zeolite pigment is to be substituted into the industry formulation to replace different pigments, to determine which combination of the porous zeolites and other pigment provides the best structural, optical, surface and print properties.

Penetration of Liquid Through Pores

The microstructure of a coated layer, including the size distribution of its micropores, is one of the most important factors, influencing the physical properties of paper including its printing characteristics (25-27). For example, print gloss and ink setting rate depend not only on the surface property of a coated paper, but also the pore size distribution of the coated layer, since it affects the rate and depth of ink absorption (28). Therefore, it is necessary to understand the porous structure of coated paper.

Absorption of liquid into the porous structure of a paper coating is one of the most important mechanisms in printing on paper substrates. When an ink comes into contact with the paper surface, the final printing results are strongly dependent on how deeply the ink penetrates in connection to the spreading on the paper, where the ink pigment particles or dyes are deposited, and in what order of time this happens. The desired balance is therefore a droplet that has the optimal spread / penetration ratio (29), sets fast within the runnability limits of the printing process, thereby depositing the color particles close to the paper surface giving a sharply defined printed dot.

In the manufacture of paper, pigments for coating and filling hold one of the key functions in the process of adsorption, spreading and absorption into the porous structure. Water transport, under the influence of external pressure, forces water to penetrate into the coating pores. Capillary transport creates water uptake through surface chemical properties. These are the primary factors involving water transport. Surface roughness, pore structure, and surface chemical properties of the coating layer influence the capillary water transport potential. The surface energy and pore size control the capillary pressure driving force. Surface roughness determines the initial water uptake.

The driving potential for the water movement is the sum of the external pressure, and the pressure difference across a curved surface called capillary pressure. The

intrusion of the liquid into the pores in response to applied pressure can be illustrated by the Young-Laplace equation (30, 31):

$$\Delta P = \frac{2 \cdot \gamma \cdot \cos\theta}{r} \qquad (i)$$

where

ΔP = pressure difference across a curved surface (capillary pressure), dyne/cm^2

γ = surface tension of liquid, dyne/cm

θ = contact angle, between liquid and solid phase, rad

r = pore radius, cm

The process of water penetration is described by Lucas and Washburn (30).

$$\frac{dL}{dt} = \frac{\gamma \cdot r \cdot \cos\theta}{4 \cdot L \cdot \mu} \qquad (ii)$$

After integrating in the range from $L_0 = 0$ to $L_1 = 1$ and from $t_0 = 0$ to $t_0 = t$, the resulting equation is

$$L^2 = \frac{1}{2} \cdot \frac{\gamma \cdot r \cdot t \cdot \cos\theta}{\mu} \qquad (iii)$$

Thus, the Lucas-Washburn equation, based on the water transport model can be written as (15):

$$L = \sqrt{\frac{2 \cdot \gamma \cdot r \cdot \cos\theta + p \cdot r^2}{4 \cdot \mu} \cdot t} \qquad (iv)$$

where:

L = length or depth of capillary penetration, cm

r = capillary radius, cm

γ = surface tension, dyne/cm

θ = contact angle, between liquid and solid phase, rad

P = external pressure, dyne/cm^2

μ = liquid viscosity, dyne-s /cm

t = penetration time, s

Therefore, when the external pressure is increased, the relative influence of the surface chemistry (capillary pressure) related forces are decreased. The surface characteristics of the coating layer influence water uptake only up to the point where the coating layer is saturated with water. When the liquid has moved through this layer, the transport rate is determined by the flow losses in the pore structure and the sorption properties of the base paper. At a high external pressure the physical structure of the pore system determines the rate factor for water penetration.

Surface Wetting Capability– Surface Energy

The wetting ability of a liquid is a function of the surface energies of the solid-gas interface, the liquid-gas interface, and the solid-liquid interface. The surface energy across an interface or the surface tension at the interface is a measure of the energy required to form a unit area of new surface at the interface. The intermolecular bonds or cohesive forces between the molecules of a liquid cause surface tension. Surface tension can be thought of as either a force per unit length or a free energy per unit area expressed as dyne/cm or ergs/cm^2. The surface tension of liquids can be measured with a Wilhelmy plate tensiometer, as well as several other techniques (31).

For example in printing processes, the ink transfer is influenced strongly by whether the liquid phase wets the paper or not. At the liquid-solid surface interface, if the molecules of the liquid have a stronger attraction to the molecules of the solid surface than to each other, the adhesive forces are stronger than the cohesive forces; then wetting of the surface occurs. Alternately, if the liquid molecules are more strongly attracted to each other and not the molecules of the solid surface, the cohesive forces are stronger than the adhesive forces; then the liquid beads-up and does not wet the surface of the part. The term surface tension is used for liquids, and surface energy for describing solids (32). The work of adhesion between a solid and liquid phase, is illustrated by the following equation (30):

$$W_{SL} = \gamma_{SV} + \gamma_{LV} - \gamma_{SL} \qquad \text{(v)}$$
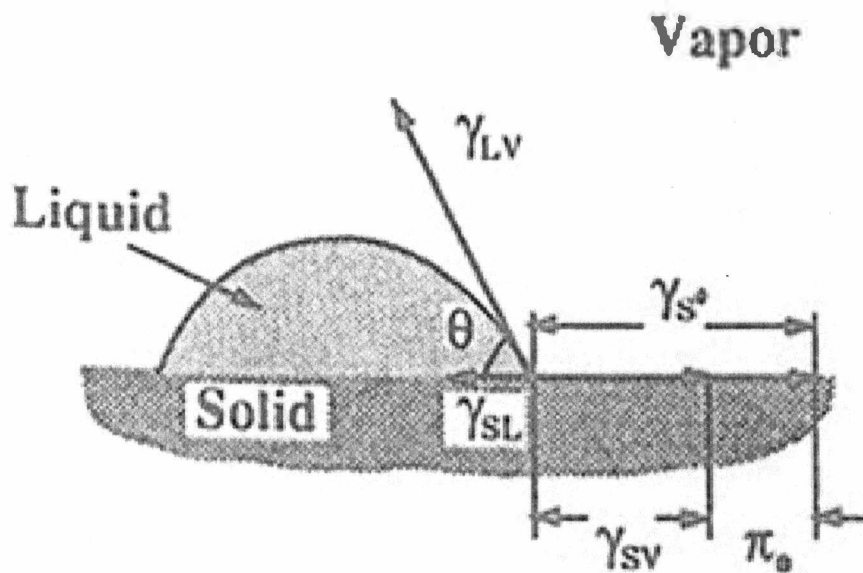
Figure 1. Components of Interfacial Tension and Contact Angle

So for a liquid to spread over the surface, the surface energy of the solid-gas interface must be greater than the combined surface energies of the liquid-gas and the solid-liquid interfaces. In gravure, it is important for the ink to transfer from the recessed cylinder cell to the substrate (to wet) and to maintain controlled spreading. The liquid may spread across the surface to form a uniform duplex film, which is a film thick enough for the two interfaces, film-air and film-solid to be independent. On the other hand, the liquid may form a drop on the solid with a finite, non-zero contact angle (33). The spreading coefficient has the significance of predicting the ink-substrate interaction. A high spreading coefficient can lead to ink penetration and feathering, and a low spreading coefficient can lead to poor ink transfer and non-uniform coverage (34). The spreading coefficient of a liquid on a solid surface, is illustrated by the equation:

$$S_{L/S} = \gamma_{SV} - \gamma_{LV} - \gamma_{SL} \qquad \text{(vi)}$$

If the spreading coefficient has a positive value or is zero, spreading will occur spontaneously; no spreading occurs if the value is negative (30, 31, 34).

The problem has been to identify both the mechanism whereby wetting influences ink transfer, and the measurable physical parameters which relate to ink transfer and printability (34). Wettability depends on four properties (a) the surface energy of paper, (b) the surface tension of the ink, (c) their interfacial tension, and (d) the equilibrium contact angle between the ink and paper, which is directly dependent on the other three factors (15). This relationship between surface tension and contact angle is given by the Young and Dupre equation (30, 34).

$$\gamma_{SV} = \gamma_{SL} + \gamma_{LV} \cos \theta \text{ or } \cos \theta = \frac{\gamma_{sv} - \gamma_{sl}}{\gamma_{lv}} \qquad \text{(vii)}$$

where:

γ_{SV} = surface energy of a solid in equilibrium with the saturated vapor

γ_{LV} = surface tension of a liquid in equilibrium with the saturated vapor

γ_{SL} = interfacial tension between the solid and the liquid

θ = contact angle, between liquid and solid phase

By combining Work of adhesion and Spreading coefficient:

$$S_{L/S} = W_{SL} - W_{LL} \qquad \text{(viii)}$$

where:

$S_{L/S}$ = Spreading coefficient of a liquid on a solid surface

W_{SL} = Work of solid-liquid adhesion

W_{SL} = Work of liquid-liquid cohesion

The contact angle measures the physical angle derived from a drop of liquid placed on a perfectly smooth solid surface. Either the liquid spreads across the surface to form a thin and uniform film, or it spreads to a limited extent and remains as a discrete drop on the surface. If the work of adhesion (solid-liquid molecules interaction) is higher than work of cohesion (liquid-liquid molecules interaction), the liquid will wet the solid. The quantitative measure of the wetting process is taken to be the contact along which the drop makes with the solid as measured through the liquid (33). A low contact angle

results from a high degree of solid-liquid interaction and a high contact angle is an indication of a low degree of interaction (30, 34). If the surface is rough, the corresponding surface area will be larger but much of it will be overshadowed by the projection since the Young equation assumes that the surface is smooth. Hence, rough surfaces change the angle as described by the Wenzel, or modified Young's equation (30, 35, 36).

$$\beta \, \gamma_{LV} \cos \theta = \gamma_{SV} - \gamma_{SL} \quad \text{or} \cos A = \beta \cos \theta \qquad \text{(ix)}$$

where:

A = apparent contact angle (degree)

β = roughness factor

θ = measured contact angle (degree)
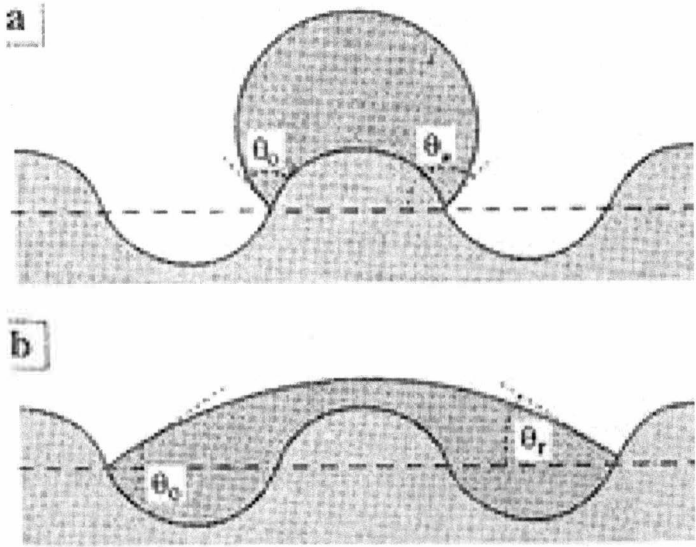
Figure 2. Cross Section of a Drop Resting on a Surface Containing a set of Concentric Grooves

Ink Transfer

When the ink contained in the cells comes into contact with the substrate, ink transfer onto the substrate as the greater surface energy of the substrate pulls the ink out of the cells. During the impression, intimate contact between the cells in the plate surface and the substrate is necessary for better ink transfer (7). The ink may penetrate into the coating pores by two mechanisms. It may be forced into the coating by the hydrodynamic pressure developed in the nip or it may be pulled into the coating by capillary forces. Whether the driving force is the hydrodynamic pressure P, or the surface tension of the ink γ, the volume of ink absorbed per unit area V, during the short impression time t, will be a function of the same structural parameters. These are the void volume fraction, or porosity ε, the average pore size r, and the tortuosity τ, defined as the average ratio of the length of the pore to its end-to-end distance (i.e. coating thickness). The relationship can be derived from the Hagen-Poiseuille and the Laplace equations, describing the respective contribution of each mechanism at a zero contact angle (37).

$$V_P = \frac{\varepsilon \cdot r}{2 \cdot \tau} \cdot \sqrt{\frac{p \cdot t}{\mu}} \qquad\qquad (x)$$

$$V_C = \frac{\varepsilon}{\tau} \cdot \sqrt{\frac{\gamma \cdot r \cdot t}{2 \cdot \mu}} \qquad\qquad (xi)$$

where:

V_P = volume of ink absorbed due to hydrodynamic pressure

V_C = volume of ink absorbed due to capillary pressure

μ = ink viscosity
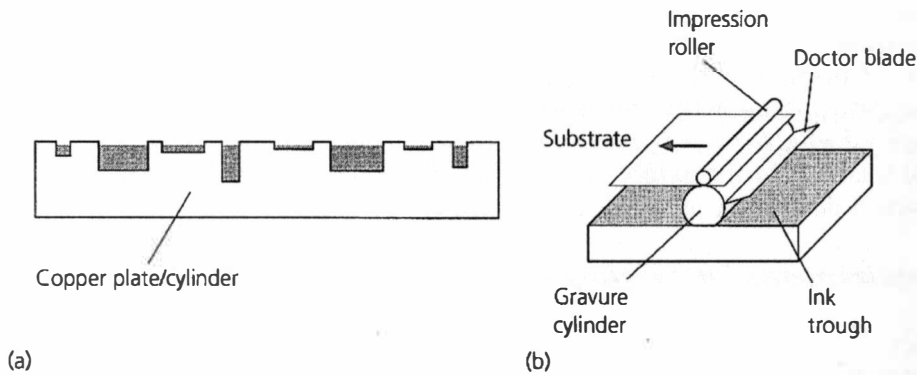
Figure 3. The Gravure Process: (a) Recessed Surface With Cells of Varying Depth and Area; (b) Printing Unit.

The pressure penetration is the overriding factor in the case of uncoated papers. However, pressure-penetration decreases faster than capillary absorption, when the pore size decreases (Equations. x and xi). The situation would then be quite different with coated papers since coating pores are one order of magnitude smaller than the pores in paper; here capillary absorption may become as important as pressure penetration.

Coating

Pigments in coating are used to improve the appearance and printability of paper. A paper coating is a composite material, consisting mainly of pigment, binder, additives and air filled voids. The void fraction of a paper coating is about 35 %, but may range from 20 % to 40 %, depending on the pigment and the properties and addition level of the binder. The void structure plays a major role in determining the optical properties, ink absorbency and ink receptivity of coated papers (38).

Zeolites- The Porous Mineral

Zeolites, aluminosilictes originally found as minerals in nature, can be synthesized with variable Si/Al ratios and variable pore sizes in various forms and have intricate cagelike labyrinths (Fig.4) with shape-and size- selective properties. Pore dimensions in the range of 0.8 to 2nm can be obtained for solids with controllable acidity associated with Al^{3+} in the silica matrix. The zeolites are also known as molecular sieves because of their properties to discriminate between molecules; they find numerous uses in separation and catalytic processes. Although they appear to be solid particles to the naked eye, they are highly porous, with a typical surface area of about 200 to 1000 m^2/g (31).

Typically forming in the cavities, or vesicles, of volcanic rocks, zeolites are the result of very low-grade metamorphism. The alumino-silicate structure is negatively charged and attracts the positive cations that reside within. Zeolites are characterized by their ability to lose and absorb water without damage to their crystal structures. The large channels explain the consistent low specific gravity of these minerals (39). Compositionally, zeolites are similar to clay minerals. More specifically, both are alumino-silicates; however, they differ in their crystalline structure. Many clays have a layered crystalline structure (similar to a deck of cards) and are subject to shrinking and swelling as water is absorbed and removed between the layers. In contrast, zeolites have a rigid, 3-dimensional crystalline structure (similar to a honeycomb) consisting of a network of interconnected tunnels and cages. Water moves freely in and out of these pores but the zeolite framework remains rigid. Another special aspect of this structure is that the pore and channel sizes are nearly uniform, allowing the crystal to act as a molecular sieve.

Suitable synthetic zeolites include, but are not limited to, the synthetic faujasite crystal types, i.e. zeolites X and Y, as well as zeolites A, L, P, Beta, synthetic mordenite

and ferrierite, ZSM-5, and MCM-22. Larger pore mesoporous silicates, such as MCM-41 and related phases, as well as other families of molecular sieves, such as aluminophosphates, silicoaluminate, aluminosilicate and titansosilicates are also suitable phases. Usually synthetic zeolites are prepared in the sodium form, that is, with a sodium cation in close proximity to each aluminum tetrahedron and balancing its charge (40).

Suitable natural zeolites include mordenite, clinoptilolite, ferrierite, dachiardite, chabazite, erionite, and faujasite.

The composition of the zeolites may vary depending on the number of tetrahedral sites that are occupied by aluminum versus silicon. The composition is usually expressed in terms of a SiO_2/Al_2O_3 ratio.
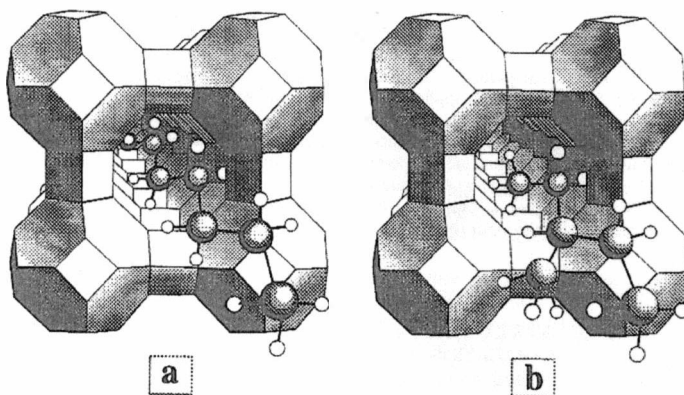
Figure 4. The Molecular Structure of a Zeolite Cage

CHAPTER III

STATEMENT OF THE PROBLEM AND OBJECTIVES

The porosity of pulp fibers and their ability to swell are of vital importance for papermaking and paper converting processes. The number and size of micro voids contribute to the macroscopic properties such as brightness, light scattering efficiency, and opacity; the swelling contributes to the development of tensile strength in paper. The fiber swelling is not however only beneficial, since it can cause dimensional and print problems in printing processes such as image distortion, fiber puffing, surface roughening, and lower print gloss. These problems make using a water-based ink with the lightweight rotogravure papers difficult.

As an industry, printers are at great risk from environmental exposure, because of potentially hazardous materials or waste, such as volatile organic compounds (VOCs). The use of water-based ink is of interest due to environmental issues with the solvent-based inks. In addition, water-based inks do not require the capital investment into explosion proof motors or solvent recovery equipment. Mottle occurs with all types of printing processes; however, it is the major set back for lightweight coated rotogravure papers due to poor wetting and ink spreading on the paper.

Incorporating zeolite, a modified clay pigment into a coating can improve the opacity, absorptive and compressibility properties of a LWC coating resulting in improved structural, optical and surface properties, and print quality of lightweight coated paper printed with water-based gravure inks.

The objectives of this study are:

(1) To incorporate a modified clay-zeolite pigment into a coating for the production of a water-based ink printed rotogravure coating.

(2) To determine the viscoelastic properties of the wet coating colors.

(3) To determine the influence on structural, optical and surface properties of the dry coating structures.

(4) To determine the influence on print quality of the coated papers printed with water-based rotogravure inks.

CHAPTER IV

EXPERIMENTAL DESIGN AND METHODOLOGY

The experimental strategy used during this research was first to investigate the properties of zeolites and second to study the surface and optical properties obtained by substituting different zeolites in a LWC rotogravure coating and their effect on final print properties printed with water based ink.

The study was further divided into seven stages: (1) screening design, (2) formulation of coating by substituting natural and synthetic zeolite pigment to a standardized LWC coating, (3) study of viscoelastic properties of coatings, (4) application of coatings onto the surface of a lightweight base sheet with a CLC, (5) evaluation of the structural, surface and optical properties, (6) printing of coated papers on a Cerutti Gravure press with water-based inks, and (7) evaluation of coating surface performance for improved printability and optics by image analysis.

Table 1, 2 & 3 gives the summary of different coating formulations that were applied on a CLC (cylindrical laboratory coater). The study plan is schematically represented in Figure 5.

Table 1

Industry Coating Formulation (C P[i])

Coating Components		Parts
PIGMENTS	Delaminated Clay (Hydraprint)	80
	Porous Zeolite (Synthetic and Natural)	0
	Calcined Clay (Ansilex 93)	8
	Titanium Dioxide (Tiona AT-1)	4
	Plastic Pigment (Dow Chemical)	8
BINDER	SBR Latex (Genflo® 5170)	6.5
X-LINKER	AZC (Ammonium Zircomium Carbonate)	1.5
LUBRICANT	Calcium Stearate (Nopcote C-104-HS)	1

Table 2

Coating Formulations With Synthetic Zeolite

Coating Components	0C8S[2] (Parts)	0T4S[3] (Parts)	0P8S[4] (Parts)	72D8S[5] (Parts)
Delaminated Clay	80	80	80	72
Synthetic Zeolite	8	4	8	8
Calcined Clay	0	8	8	8
Titanium Dioxide	4	0	4	4
Plastic Pigment	8	8	0	8
SBR Latex	6.5	6.5	6.5	6.5
AZC	1.5	1.5	1.5	1.5
Calcium Stearate	1	1	1	1

Table 3

Coating Formulations With Natural Zeolite

Coating Components	0C8N[6] (Parts)	0T4N[7] (Parts)	0P8N[8] (Parts)	72D8N[9] (Parts)
Delaminated Clay	80	80	80	72
Natural Zeolite	8	4	8	8
Calcined Clay	0	8	8	8
Titanium Dioxide	4	0	4	4
Plastic Pigment	8	8	0	8
SBR Latex	6.5	6.5	6.5	6.5
AZC	1.5	1.5	1.5	1.5
Calcium Stearate	1	1	1	1

[1]CP - control coating or industry formulation

[2]0C8S - substitution of calcined clay with synthetic zeolite

[3]0P8S - substitution of plastic pigment with synthetic zeolite

[4]0T4S - substitution of titanium dioxide with synthetic zeolite

[5]72D8S - substitution of delaminated clay with synthetic zeolite

[6]0C8N - substitution of calcined clay with natural zeolite

[7]0P8N - substitution of plastic pigment with natural zeolite

[8]0T4N - substitution of titanium dioxide with natural zeolite

[9]72D8N - substitution of delaminated clay with natural zeolite

```
┌─────────────────────────┐
│   COATING FORMULATION   │
│        PIGMENTS         │
│        BINDERS          │                    ┌──────────────────────────────┐
│        ADDITIVES        │                    │                              │
└─────────────────────────┘                    │ ▷DYNAMIC STRESS SWEEP        │
             │                                 │ ▷FREQUENCY STRESS SWEEP      │
             ▼                                 │ ▷STEADY STRESS SWEEP         │
┌─────────────────────────┐                    │                              │
│                         │───────────────────▶│                              │
│      VISCOELASTIC       │                    │                              │
│   PROPERTIES TESTING    │                    └──────────────────────────────┘
└─────────────────────────┘
             │
             ▼
┌─────────────────────────┐                    ┌──────────────────────────────┐
│          CLC            │                    │ ▷PORE SIZE AND VOLUME        │
│         COATER          │                    │ ▷WATER PENETRATION           │
└─────────────────────────┘                    │   CHARACTERISTICS            │
             │                                 │ ▷CONTACT ANGLE               │
             ▼                                 │                              │
┌─────────────────────────┐                    │ ▷SMOOTHNESS                  │
│                         │                    │ ▷COMPRESSIBILITY             │
│     SUPER CALENDER      │───────────────────▶│ ▷GLOSS                       │
│                         │                    │                              │
└─────────────────────────┘                    │ ▷BRIGHTNESS                  │
             │                                 │ ▷OPACITY                     │
             ▼                                 │                              │
┌─────────────────────────┐                    └──────────────────────────────┘
│   STRUCTURAL, SURFACE   │
│  AND OPTICAL PROPERTIES │◀───────┘
│         TESTING         │
└─────────────────────────┘
             │
             ▼
┌─────────────────────────┐                    ┌──────────────────────────────┐
│  CERUTTI PRESS PRINTING │                    │                              │
│  OF COATED PAPERS WITH  │───────────────────▶│                              │
│    WATER-BASED INKS     │                    │ ▷PRINT GLOSS                 │
└─────────────────────────┘                    │ ▷OPTICAL DENSITY             │
             │                                 │ ▷IMAGE ANALYSIS- DOT AREA,   │
             ▼                                 │ PERIMETER AND ROUNDNESS      │
┌─────────────────────────┐                    │                              │
│                         │                    │                              │
│  PRINTABILITY ANALYSIS  │                    │                              │
│                         │                    └──────────────────────────────┘
└─────────────────────────┘
```

Figure 5. Flow Chart of the Experimental Plan

Screening Design

First, it was necessary to characterize the different zeolites based on their brightness, surface area and particle size. The specific surface area and micropore volume were studied by using a micrometrics TriStar 3000™ instrument. This analyzer uses physical adsorption and capillary condensation principles to obtain information about the surface area and porosity of a solid material. These data are extremely important to select the appropriate zeolite pigments. Based on these results, two different grades of zeolite pigment were selected for further study.

The coating colors were prepared by substituting zeolite and SBR binder at different pigment to binder ratios in a typical commercial formulation. Drawdowns with Meyer rods were performed to determine at what pigment to binder ratio dusting would begin, in order to determine the minimum level of binder required. A Taber Abrasion Test was used to determine the abrasion resistance of the coating.

Coating Preparation

To start, a formulation for an industrial coating for a lightweight coated paper is needed. The industry coating formulation can be found in Table 1. The synthetic and natural zeolite pigments were added to the industry formulation to examine the effects on rotogravure printability. The independent variable in the experiment will be the substitution of porous pigments to the industry coating formulation.

Styrene-Butadiene latex (SBR), supplied in a slurry form at 50 % solids and 7.3 pH, was used as a binder to impart gloss, binding strength, solvent resistance & less print mottle. The additives (a) aluminum zirconium carbonate (AZC) insolubilizer supplied in slurry form at 40 % solids was used to impart water resistance, (b) calcium stearate

lubricant supplied in slurry form at 50% solids was used to improve flow properties of the coatings.

Each of the coatings was made at 58-60 % solids by first dispersing the dry pigments in water under high shear. After adding lubricant, the pH was adjusted to 8.0 with NH_4OH. The binder will then was added to the pigments under mild agitation and the viscosity of the coating was measured using a Brookfield DV-III viscometer. The formulations for the varied formulations can be found in Tables 2 & 3.

<div align="center">Viscoelastic Properties of Coating</div>

The rheological properties of the coatings were measured to determine the influence of porous zeolite on wet coating structure. Dynamic rheological measurements were performed using a Dynamic Stress Rheometer. Different tests were conducted, such as dynamic stress sweep (DSS), frequency stress sweep (FSS), and steady stress sweep (SSS) tests.

Dynamic Measurements

Dynamic measurement has been used widely in studying the viscoelastic properties of coating colors. Dynamic measurement requires an instrument that can generate sinusoidal stress or strain as an input to the fluid under test and record the strain or stress resulting from the fluid deformed as an output (41). Values of storage modulus, G', loss modulus, G'' and dynamic viscosity, η', are obtained. The storage modulus gives information about the elastic character of the fluid or the energy storage that takes place during the deformation. The loss modulus gives the information about the viscous character of the fluid or the energy dissipation that occurs in flow. The phase angle δ between stress and strain is normally represented by the loss tangent, $\tan \delta$. The complex modulus, G^*, and complex viscosity, η^* (or equivalently the real and imaginary parts of the complex) can also be determined (42).

In this experiment, the material is subjected to sinusoidally variable stress (at a constant frequency), which is systematically increased, and the sinusoidal strain response is measured. At low stresses the material will behave in a linear manner, i.e. the strain is proportional to stress; while at higher stresses the response will be non-linear. The extent of the linear region will provide information on both the microstructure and performance characteristics.

Dynamic Frequency Measurements

The FSS was performed at a stress in the linear region just before the critical stress value obtained from the DSS. In this experiment the material is subjected to a small constant applied stress over a given frequency range. The slope of G' and G" as a function of frequency will give information about the microstructure of the material.

Steady Shear Measurements

Rheological experiments under steady shear were performed using "viscoelastic flows" that are indistinguishable from simple steady flow for all practical purposes. From a steady-shear flow experiment, three material functions can be measured viz., the viscosity (η), and the first and second normal stress coefficient (ψ_1 & ψ_2). Among these, the viscosity is the simplest and most important material function and can be calculated from the measured shear stress, and the applied shear rate. Four types of behavior can be distinguished: Newtonian, shear thinning, yield stress (followed usually by shear thinning), and shear thickening. A plot of viscosity versus shear rate or shear stress is called a flow curve (42).

In this experiment, a shear stress is applied to the material and the resulting shear rate is measured. The stress is increased stepwise during the experiment and the viscosity calculated at each stress. In steady shear, the material functions are always obtained under flow conditions that corresponds to relatively drastic deformation. Consequently, the

microstructure under steady flow will be very different from the microstructure under static conditions. These tests were performed at 25^0C with couette geometry.

Coating Application - Cylindrical Laboratory Coater

Once each of the formulations was made, the coatings were applied onto a commercial rosin-sized lightweight basesheet using a Cylindrical Laboratory Blade Coater (CLC). After coating, the coat weight was determined by direct weighing and was maintained at $5.6 - 5.8$ g/m^2. The coated samples were cut to 8 by 24 inches. The samples were then calendered at 2000 PLI to get the desired smoothness by passing the samples twice through a soft nip supercalender.

Structural, Surface and Optical Properties

The coated papers were conditioned at 50 % RH and 73^0 F before testing for (a) the structural properties, coating pore size and volume, contact angle, and water penetration characteristics; (b) the surface properties, gloss, smoothness and compressibility; and (c) the optical properties, brightness, and opacity.

The coating pore size and volume was measured using Mercury Intrusion Porosimeter (MIP). MIP is a technology designed to measure the total volume, and size distribution of the inter particle / intra particle void space (26, 43). The mercury intrusion porosimeter functions by forcing mercury (Hg), a non-wetting liquid, into the pores of a sample at a specified and controlled pressure points. As the pressure is increased, Hg intrudes progressively into smaller void capillaries. Intruded Hg only fills pores for which the applied pressure is greater than the tension forces of the surface meniscus. Hg porosimeter can measure pore size from 4 nm to 360 μm and pressure ranges from 0 to 60,000 psia.

The liquid penetration into the paper surface was analyzed based on the contact angle and dynamic penetration measurement. The contact angle was measured by a First Ten Angstrom Dynamic Contact Angle Tensiometer. The Emco Dynamic Penetration Measurement (DPM 30) with DPM software version 3.3 was used for the study of liquid penetration in to the paper coating. For the measurement, the transmitter generated 2 MHz ultrasound wave. After passing through the sample, the ultrasound wave arrived attenuated at the receiver. The loss of intensity measured and then processed in the PC with a millisecond cycle.

The GE Brightness of paper was measured using a Technidyne brightness meter, TAPPI procedure T452 om-87. Opacity was measured with a BNL-2 Opacimeter using the TAPPI method T425 om-86. The Gloss was measured with a Hunter 75^0 Glossmeter, using the TAPPI method T480 om-82.

The surface smoothness/roughness of all samples were measured with a Parker Print-Surf roughness tester Model ME-90 (Messmer Instruments Ltd., U.K.) at 500 and 1000 kPa clamping pressure using the TAPPI method T555 pm-94. The compressibility was calculated as the ratio of roughness at 500 kPa and 1000 kPa clamping pressure. The air permeability/porosity of all samples were measured with a Parker Print-Surf roughness tester Model ME-90 (Messmer Instruments Ltd., U.K.) at 1000 kPa clamping pressure using the Parker Print Surf method.

Printing Application – Cerutti Gravure Press

The printing of each coated samples were carried out at 350 ft/min on a Cerutti pilot rotogravure printing press (Cerutti Model 118, Casale Monferrato, Italy) with water-based gravure ink. An Electromechanically engraved gravure cylinder of 35.99 in circumference and 11.459 in diameter with various volumetric and cell configurations was used. The CLC coated sheets were printed by drop-in method. The 8" by 24" sheets

were taped to web and drop in pinch point i.e. in between impression roll and printing cylinder. A commercial alkaline black water-based ink was used at a viscosity of 24 seconds, measured with a number No. 2 Shell efflux cup. The water-based ink has a pH of 9.0, and solids content of 55%.

Printability Analysis – Image Analyzer

Finally, the print quality of the coated papers was measured and correlated with the coated paper properties. The following print properties were measured: (a) print gloss, optical density and print contrast; (b) Image analysis- dot area, roundness, and perimeter. Image Analysis of printed samples dots was measured at 5 % tone step by a Hitachi HV-C 10 camera (Hitachi Denshi, Ltd., Japan). Computer software Image ProPlus, Version 4.0, was used for data processing. Image analysis served to quantify the individual dot attributes (44). For testing the ink gloss, the same Glossometer was used as for paper gloss testing, but at an angle of 60^0. Optical density was measured with an X-Rite 408 Densitometer.

After all the experiments were conducted, the data were analyzed. From the observations of the tests used, recommendations for improvements were made.

CHAPTER V

RESULTS AND DISCUSSION

The main objective is to study the influence of modified clay zeolite pigment on structural, surface, optical and printing properties of a LWC rotogravure coating printed with water based inks. All data with standard deviations are included in the appendix section of this report.

Zeolite Screening Phase

For different zeolite pigments including conventional coating pigment, specific surface area and micropore volume were studied by using the TriStar 3000™ instrument. An overview of pigment particles internal, external and specific surface area and micropore volume of the current coating pigments and the new pigments; zeolites (synthetic and natural) are shown in Table 4. The synthetic zeolite shows significantly higher BET surface area over the other pigments. The BET surface area of pigments depends on their internal porosity and particle size.

Table 4

BET Surface Area of Different Coating Pigments

Pigments	BET Surface Area (m^2/g)	Micropore Area (m^2/g)	External Surface Area (m^2/g)	Micropore Volume (cm^3/g)
Delaminated Clay	14.80	1.59	13.21	0.00072
Calcined Clay	14.23	1.16	13.07	0.00052
Titanium Dioxide	11.17	0.30	11.47	0.00025
Synthetic Zeolite	675.94	606.26	69.68	0.28000
Natural Zeolite	41.25	6.52	34.73	0.00260

Binder Optimization

The different coated sheets obtained from laboratory drawdowns by substituting zeolite and SBR binder at different pigment to binder ratios in an industry formulation were evaluated for dusting. Visual evaluations as well as the Taber Abrasion Test, were performed to determine the minimum level of binder required.

The Taber Abrasion Test (TAT), which treats a sample on a turntable with the surface being rubbed by a moving paintbrush, determines the abrasion resistance of the paper-coating surface. The amount of coating removed in a set time frame is expressed by weight in grams. Table 5 shows that coating #D has lowest coating removal from the surface. From both Taber Abrasion Loss and visual evaluation, the coating # D with 6.5 parts SBR binder gives the best results.

Table 5

Binder Optimization Taber Abrasion Loss Results

Coating Components	# A	# B	# C	# D	# E	# F	# G
Delaminated Clay	72	72	72	72	72	72	72
Synthetic Zeolite	16	16	16	16	16	16	16
Calcined Clay	8	8	8	8	8	8	8
Titanium Dioxide	4	4	4	4	4	4	4
Plastic Pigment	8	8	8	8	8	8	8
SBR Latex	4.0	4.8	5.6	6.5	7.2	8.0	9.6
AZC	1.5	1.5	1.5	1.5	1.5	1.5	1.5
Calcium Sterate	1	1	1	1	1	1	1
Abrasion Loss (wt/1000 rev)	0.102	0.048	0.048	0.039	0.042	0.041	0.43

Rheological Properties

The following rheological plots are referred to the nine different coatings used in this study. Figure 6 shows representative storage modulus G' curves for different coating formulations as a function of shear stress. The storage modulus of all samples, including a control sample without zeolite approached similar values except coating 72D8N at high shear stress. Comparing Figures 6 and 7, we see that the elastic modulus is higher than loss modulus for all coatings. This implies that all the coatings are predominantly elastic in nature. From Figure 6 it is clear that the coatings with synthetic zeolite shows more linear viscoelastic region over the coatings with natural zeolite. This implies that the synthetic zeolite coatings pigment particles are more dispersed and have less tendency towards sedimentation.

Figure 8 and 9 shows the dynamic rheological response of the coating as a function of frequencies. The storage modulus becomes larger than the loss modulus at high frequency, but remains smaller at low frequencies. Both quantities show a weaker dependence on frequency, with lower slope in terminal zone. Thus, dynamic rheology shows the viscoelastic nature of these systems as they exhibit comparable elastic and viscous character. The viscosity of a flocculated dispersion greatly exceeds the viscosity of a non-flocculated system. Hence, in this dispersion, where the interparticle forces are strong, there will be a tendency for the particles to adhere to one another and form large structures called aggregates or flocs.

Figure 10 shows representative viscosity curves for different coating formulations as a function of shear stress. The viscosity of all samples, including a control sample without zeolite increases over a certain range of shear stress until it reaches a maximum value. This shows the shear thickening behavior of the coatings. Moreover, as shear stress

increases the viscosity decreases attaining a constant value and this shows the shear-thinning behavior of the coatings. The viscosity starts decreasing for all coating at high shear stress. This shows the shear-thinning behavior of the coating formulations. All the coatings also show the yield stress. Shear thinning and yield stress behavior typically signifies the presence of a particulate network structure in the system at rest and the shear induced breakdown of the network in to individual particles. The most significant factors that influences measured shear flow properties are molecular composition and structure. The molecular weight distribution influences the shape of the viscosity function. The transition between the constant zero shear thinning is more abrupt and occurs at high shear rate for narrow molecular weight distribution material than for the broadly distributed material.

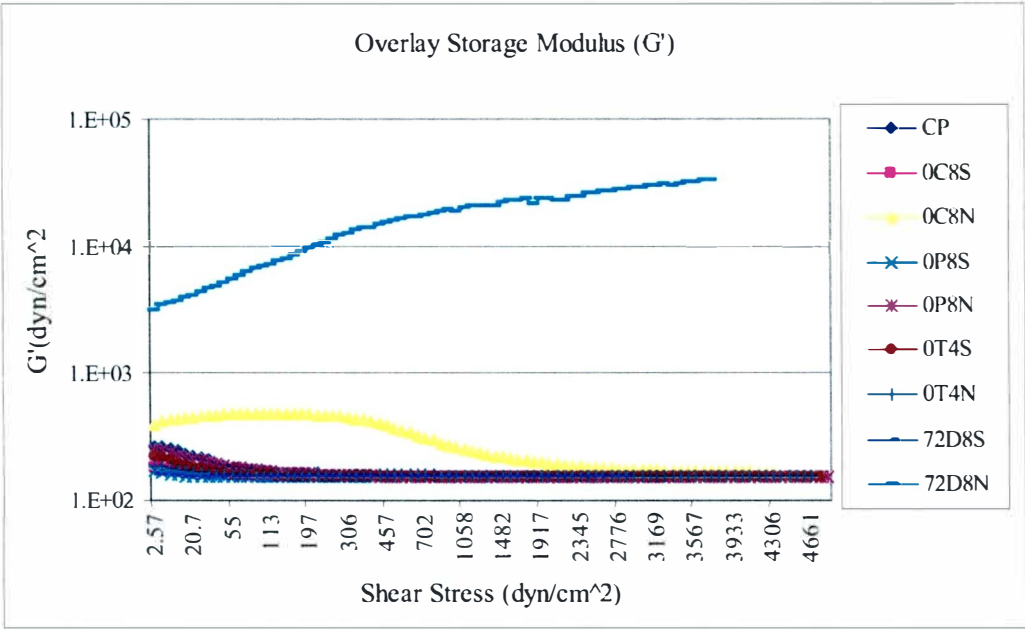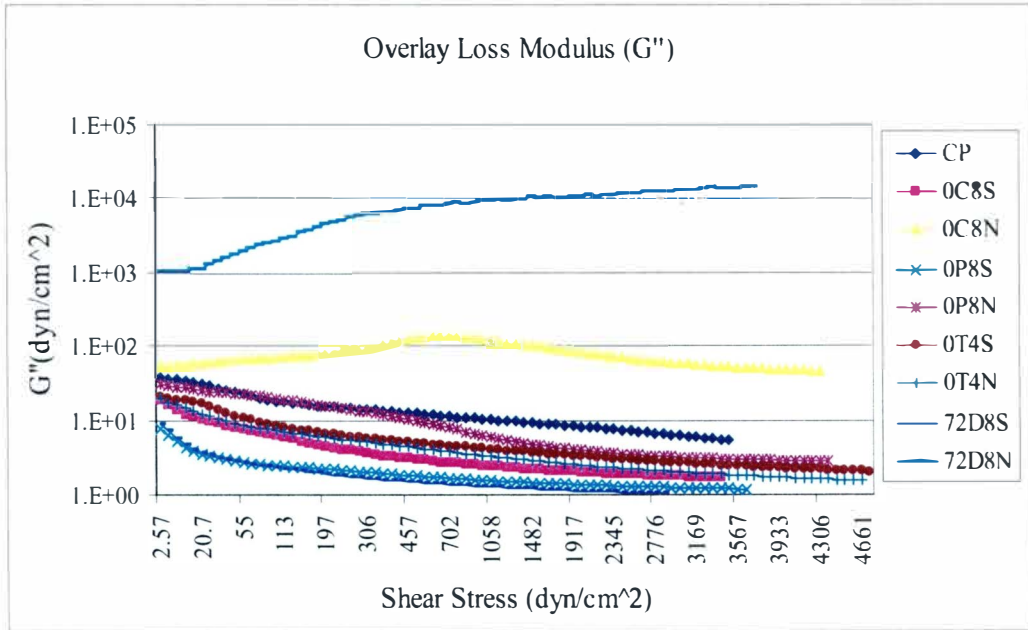Figure 6. Storage Modulus (G') as a Function of Shear Stress of Different Coatings

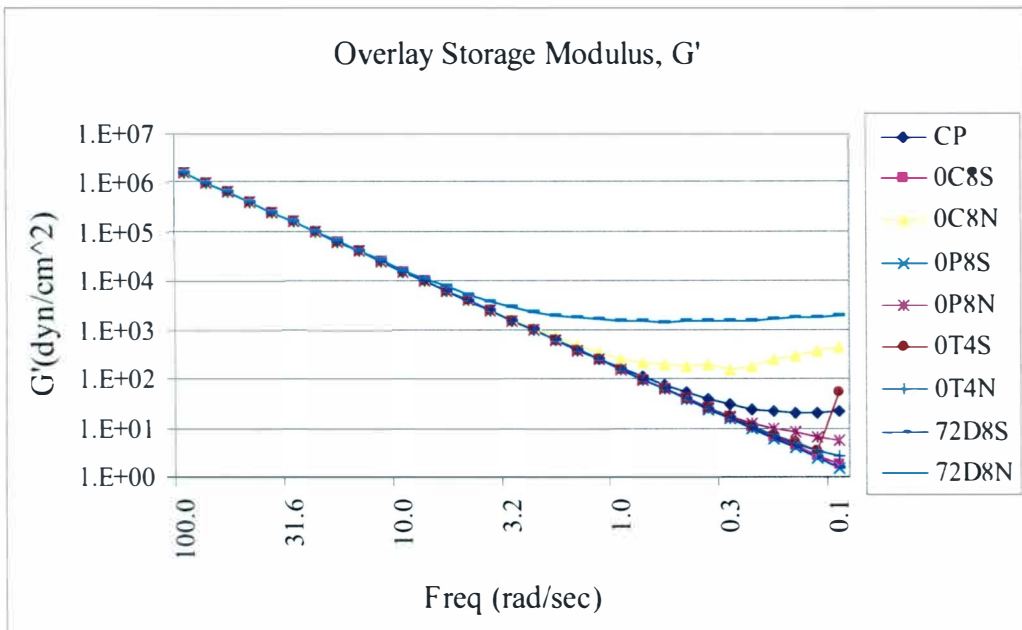Figure 7. Loss Modulus (G") as a Function of Shear Stress of Different Coatings

Figure 8. Storage Modulus (G') as a Function of Dynamic Frequency of Different
Coatings
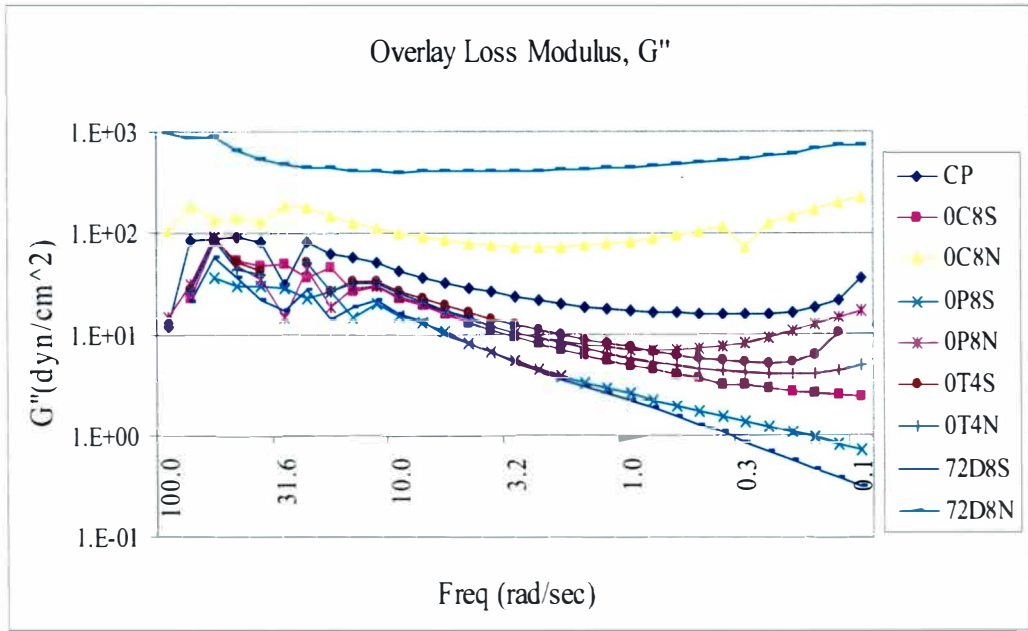
Figure 9. Loss Modulus (G") as a Function of Dynamic Frequency of Different Coatings
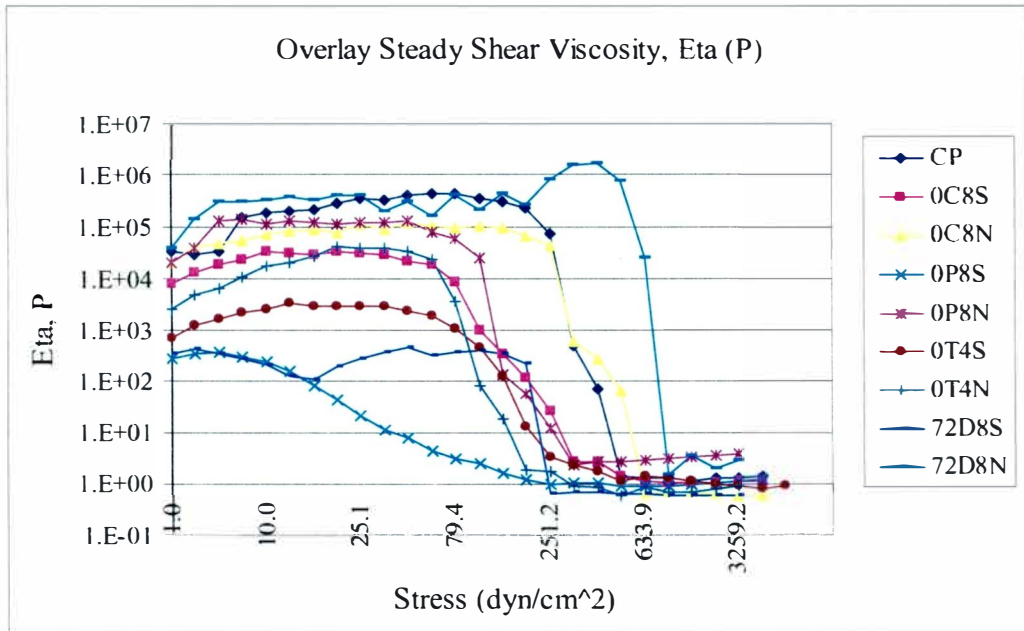
Figure 10. Steady Shear Viscosity, (η) as a Function of Shear Stress of Different Coatings

Structural Properties

Porosimetry and Permeability

Mercury intrusion porosimetry is used to investigate the structure of the coated papers. The porosimetry and the mean pore diameter were evaluated on both the coating layer and the base paper beneath the coating layer.

Table 6 shows the influence of zeolite pigment on the porosity of the coated papers. The intrusion volume represents the amount of mercury required to completely fill the pores within the paper. Hence, the higher the intrusion volume, the more porous is the coating layer. Coating 0T4S has highest intrusion volume followed by coating 0P8S. Although some of the coating with zeolite has higher intrusion volume over the control coating, there is little difference among the different samples.

Table 6

Mercury Intrusion Porosimeter Results of Different Coatings

Coatings	Total Intrusion Volume, mL/g	Pore Diameter (μm)	Total Pore Area (m^2/g)
BASE	1.8831	0.0057	9.574
CP	1.3492	0.0054	18.493
0C8S	1.1881	0.0045	98.796
0C8N	1.4508	0.0060	62.106
0P8S	1.4860	0.0669	4.760
0P8N	1.4810	0.0052	20.298
0T4S	1.8535	0.0052	62.686
0T4N	1.0002	0.0045	20.209
72D8S	1.0949	0.0040	84.991
72D8N	1.3002	0.0059	12.948

Dynamic Contact Angle

Liquid penetration into the paper surface was analyzed by measuring the contact angle and video was recorded with a high-speed camera (200 frames/sec) over period of 10 seconds. A computer program calculates the contact angle θ, the diameter d, and the profile surface S of the drop are recorded from 0 to 9 seconds. The θ, h, and S values decrease with the contact time. Inversely, the slope is positive for the drop diameter d. The surface S of the drop profile is directly related to the drop volume, if evaporation is neglected over the very short times involved. The decrease of S represents the liquid penetration into the paper. The drop diameter d represents the liquid spreading.

Figure 11 shows the graphical representation of contact angles measured by using water with the First Ten Angstrom Dynamic Contact Angle Tensiometer. The decrease in the contact angle is recorded for all the nine coated papers and base paper over the time, as represented in Figure 11. For the control coated paper, the average contact angle θ value is 60^{0}. For the coated papers with synthetic zeolite, the average contact angle θ value is between 63^{0} and 69^{0}. For the coated papers with natural zeolite, the average contact angle θ value is between 37^{0} and 60^{0}.

The decrease in contact angle θ originates from the two phenomena of the water penetration into the paper and the drop spreading over the paper. Both the surface properties and the permeability properties are influencing the water behavior over the coated paper surface. The behavior of water drop on a paper depends both on the paper permeability and on the paper roughness.

Figure 12 shows the contact angle confidence data. The results show that uncoated base paper gave the highest contact angle followed by 0C8S. The 0P8N gave the lowest contact angle. All the samples show the small confidence interval. The small confidence interval indicates that the results can be trusted.
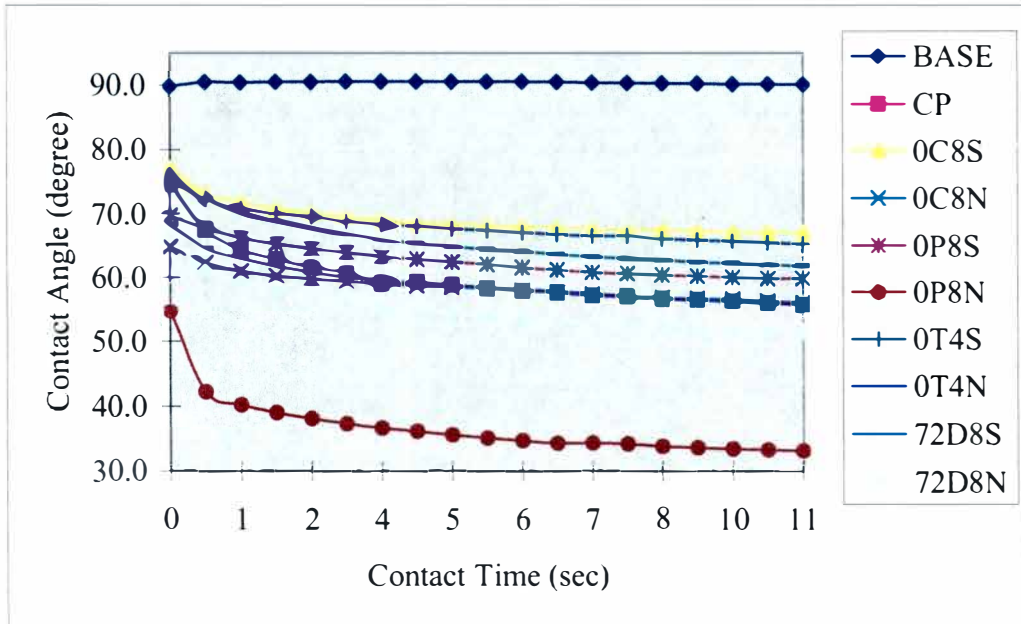
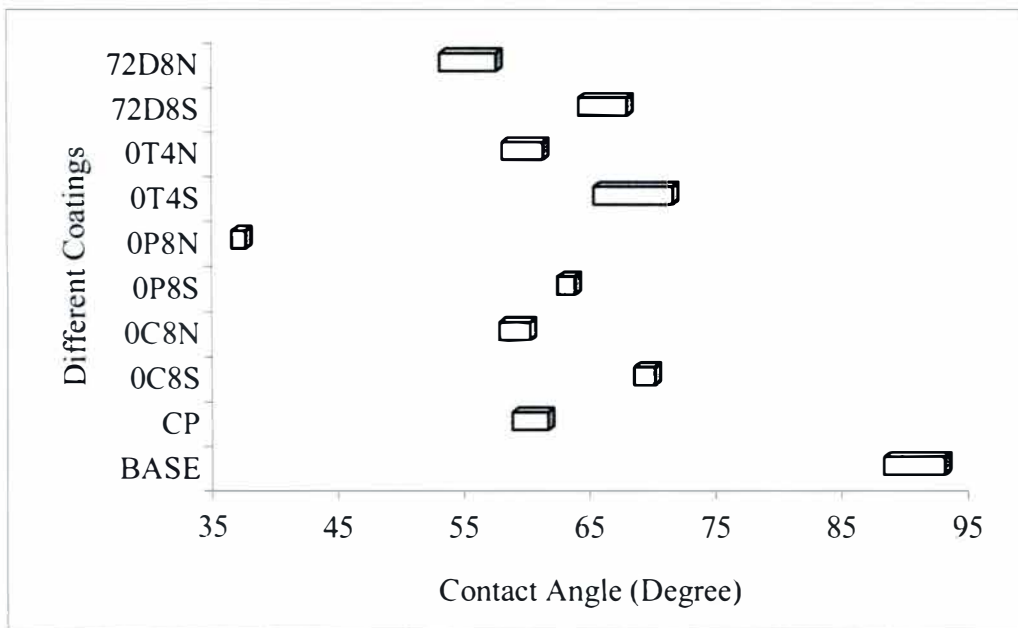Figure 11. Contact Angle Versus the Contact Time of Different Coatings

Figure 12. Contact Angle Confidence Level as a Function of Different Coatings

Ultrasound Absorption

The principle of ultrasound absorption is based on the fact that liquid conducts sound faster and better than air. Therefore, when the absorption of ultrasound through a sheet is measured while this sheet is being wetted, a wetting curve is observed.

Samples were tested for ultrasound absorption while being wetted by water. From the output graph, two kinds of information are available: first, the time that it takes the liquid to penetrate into the pores, and, second, the wetting curve. As can be seen in Figure 13, transmittance increases with time to a certain level. After this level, transmittance significantly decreases to the point where it does not change with time any more. The first transmittance increase is due to penetration of the water into the fibers. Air, that is present in the voids, has low ultrasound conductivity, and thus while being replaced by water, which has higher ultrasound conductivity, transmittance increases. The time, t_{max}, (Figure 13) is the time of the maximum transmittance; it represents the time needed for the water to replace all air voids, and thus is the maximum penetration point. After this point is reached, water starts to interact with fibers and wetting occurs. Fibers are being released and loosed, which results in lower transmittance. The curve reveals how fast fibers absorb the water.

The time that can be observed from these curves is a very important variable in the Lucas-Washburn equation. The most important factor when dealing with absorption studies is that liquid absorption during the first few seconds is absolutely critical, because of the ink penetration during printing and converting.

To understand the wetting phenomena, control and different samples, coated with and without zeolite including base sheet, were compared. Figure 14 shows the wetting curves for these sheets. As can be observed from this figure, the basesheet has a very steep slope and the curve reaches a constant value within 10 seconds. All the coated

samples including control showed similar absorption. The coated sample with synthetic zeolite has lower absorption compared to control and coated samples with natural zeolite. Figure 15 shows the wetting curve for the sample coated with synthetic zeolite pigment. The coating 0P8S shows faster absorption over the other coatings. Figure 16 shows the wetting curve for the samples coated with natural zeolite pigment. The coating 0P8N shows faster absorption over the other coatings.
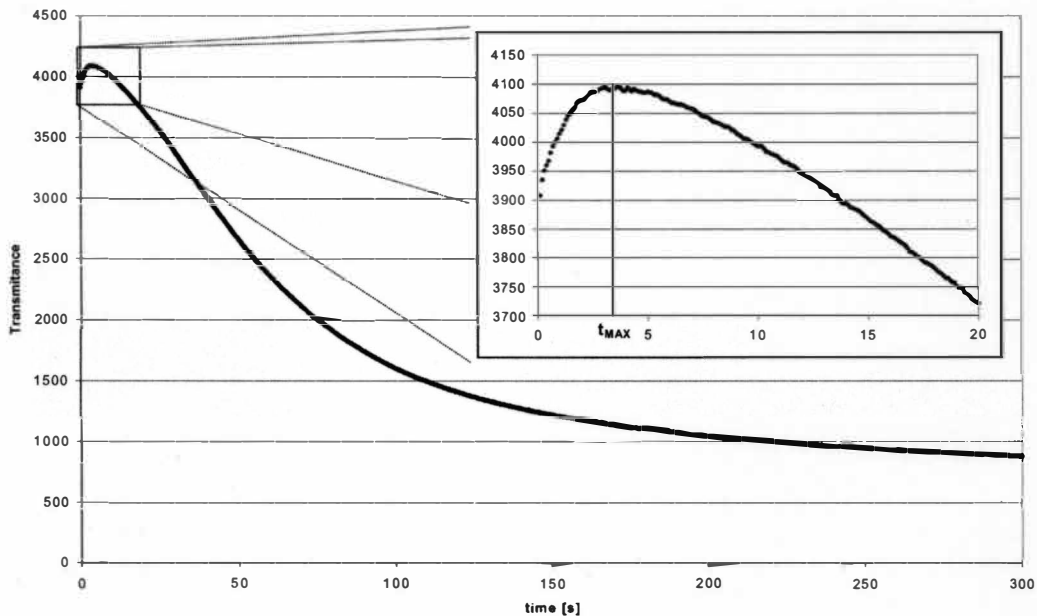
Figure 13. Ultrasound Transmittance Versus Time of Liquid Penetration

For all coatings, there were no significant differences in the slop of the curve at long period (Figure 14-17). But at short times, the curves of natural zeolite coatings decreased rapidly. It is believed that the fibers swelled more, because the bigger porous structure of the natural zeolite coatings absorbed liquid faster.

40
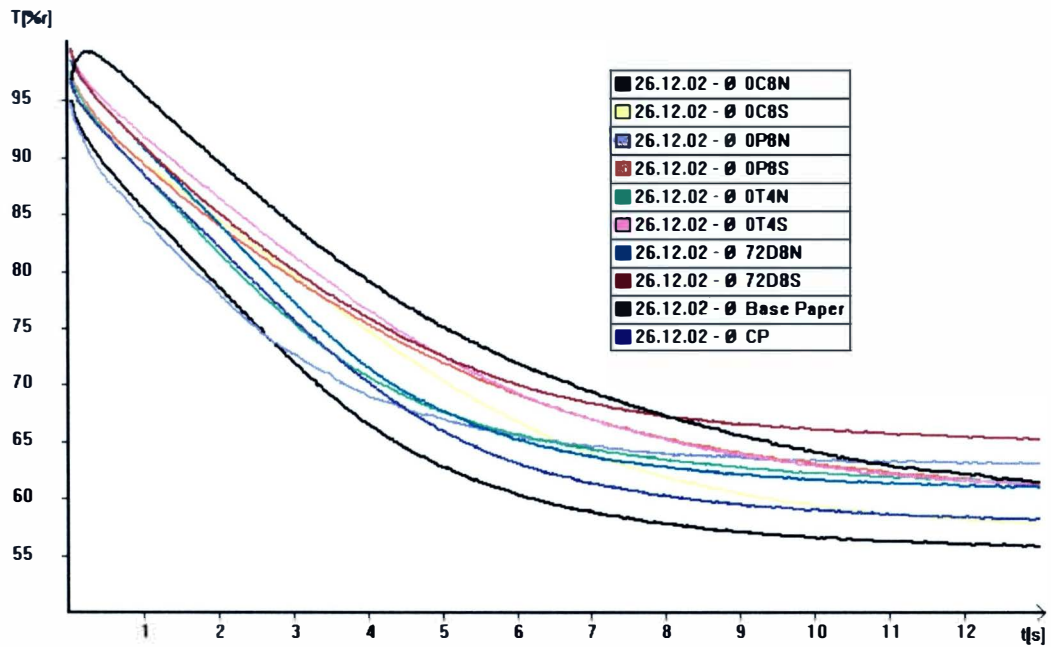
Figure 14. Ultrasound Transmittance Curve of Different Coating and Base Paper
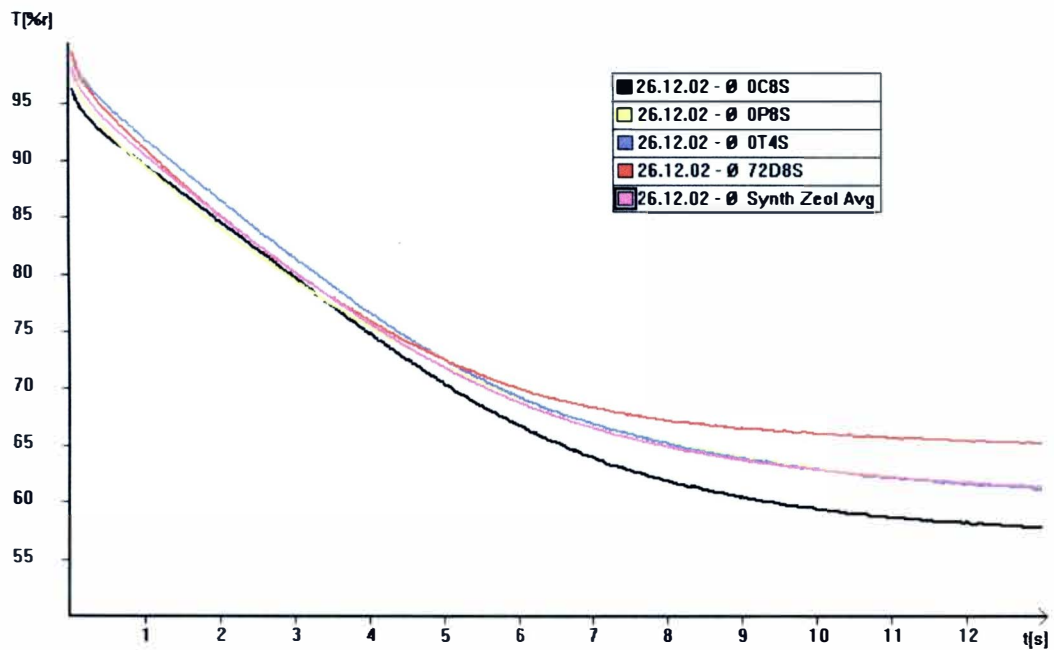
Figure 15. Ultrasound Transmittance Curve of Coated Paper With Synthetic Zeolite

41
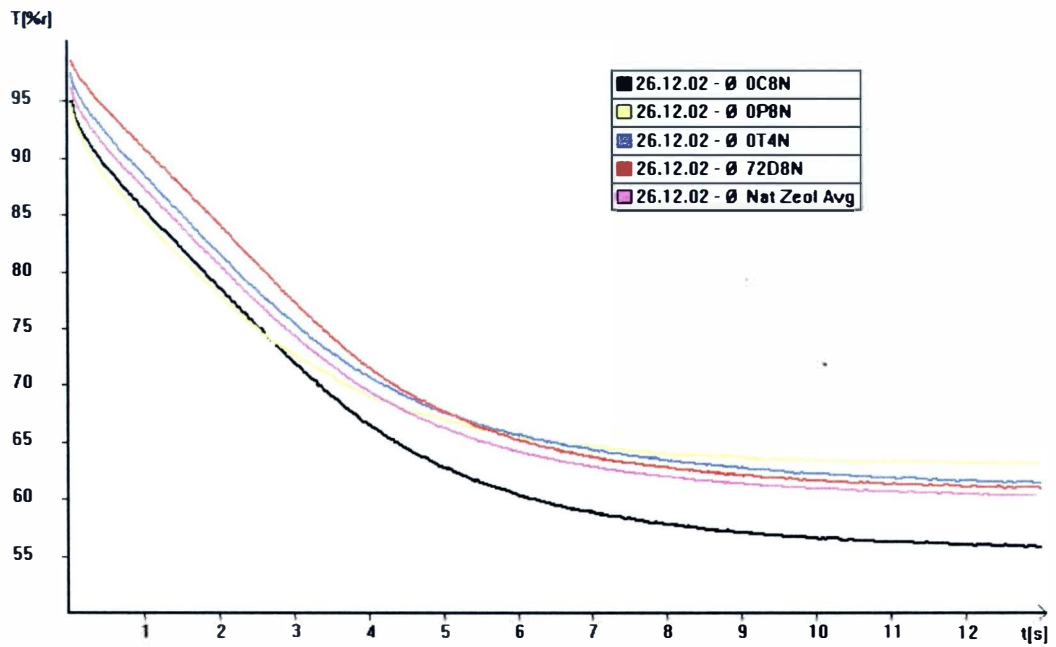
Figure 16. Ultrasound Transmittance Curve of Coated Paper With Natural Zeolite
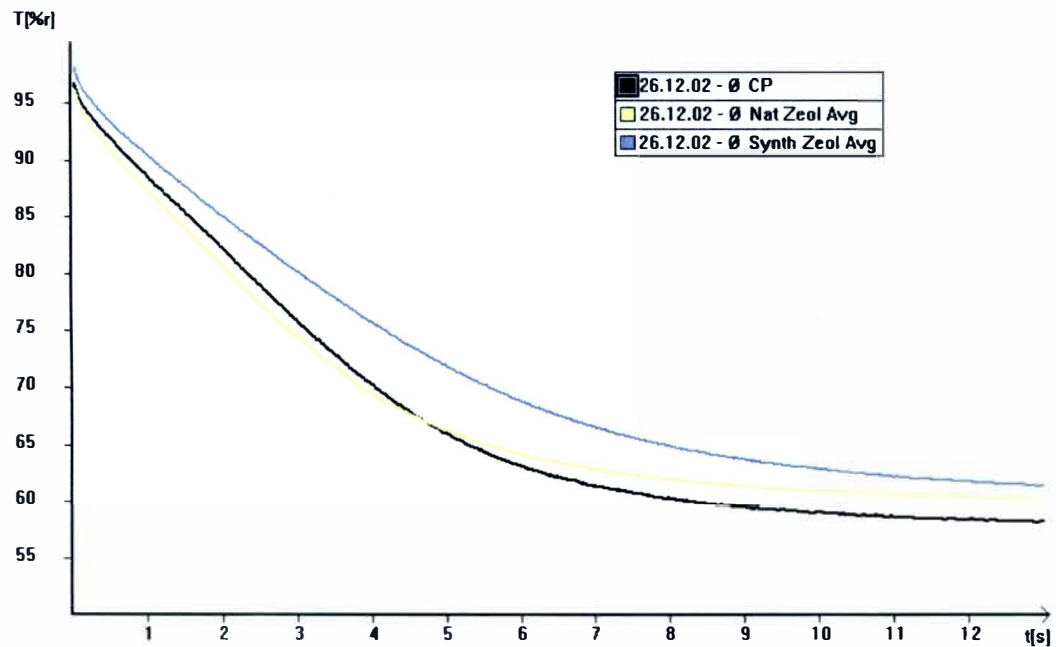
Figure 17. Ultrasound Transmittance Average Curve of Control, Synthetic & Natural Zeolite Coatings

42

Optical Properties

Tables 7 summarize the optical properties for the industry and eight different coatings with zeolite pigments. According to data collected from this experiment, the modified clay pigment did improve the optical properties of paper. The optical properties of the control formulation produced results close to current industry standards. Optical properties currently in use for a LWC matte rotogravure coating have; GE brightness from 69 to 72 %, opacity from 82 to 92 %, and gloss from 40 to 45 %. Brightness and opacity are especially important for the light weight coated papers. This is related to the fact that the coat weights are getting lighter however a better coverage is necessary to reach the expected goals.

Table 7

Comparison of Optical Properties of Different Coatings

Coatings	GE Brightness (%)		Opacity (%)		Gloss 75^0 (%)	
	Avg.	STD	Avg.	STD	Avg.	STD
CP	70.70	0.20	81.99	0.68	43.30	1.74
0C8S	71.10	0.40	80.91	0.56	50.80	5.22
0C8N	71.50	0.30	82.87	0.51	50.10	3.98
0P8S	72.50	0.20	82.62	0.54	43.00	4.68
0P8N	70.60	0.50	82.66	1.07	39.80	1.73
0T4S	71.70	0.30	81.79	0.98	47.10	4.20
0T4N	71.40	0.20	81.63	0.53	45.90	4.30
72D8S	71.30	0.20	82.60	1.13	49.30	1.19
72D8N	72.60	0.20	82.17	0.94	47.80	2.58

According to the collected data, when compared to the industry standard, the 72D8N and 0P8S coatings had the best brightness and opacity results as represented in Figure 18 and 19. The increased brightness and opacity can be attributed to the shape and properties of the modified clay zeolite pigment particles. The air pockets similar to sponge with zeolite particles cause voids in the coating so when light is reflected onto the surface of the sheet increased scattering occurs, raising the brightness and opacity of the coated sheet.

Gloss is not as important to a matte coating but it was tested also as shown in Figure 20. The porous zeolite also offers higher gloss alongside both brightness and opacity. The coating 0C8S gave the highest gloss followed by coating 0C8N. If higher gloss is not needed, additional brightness and opacity can be gained by reducing the pressure on the calender.
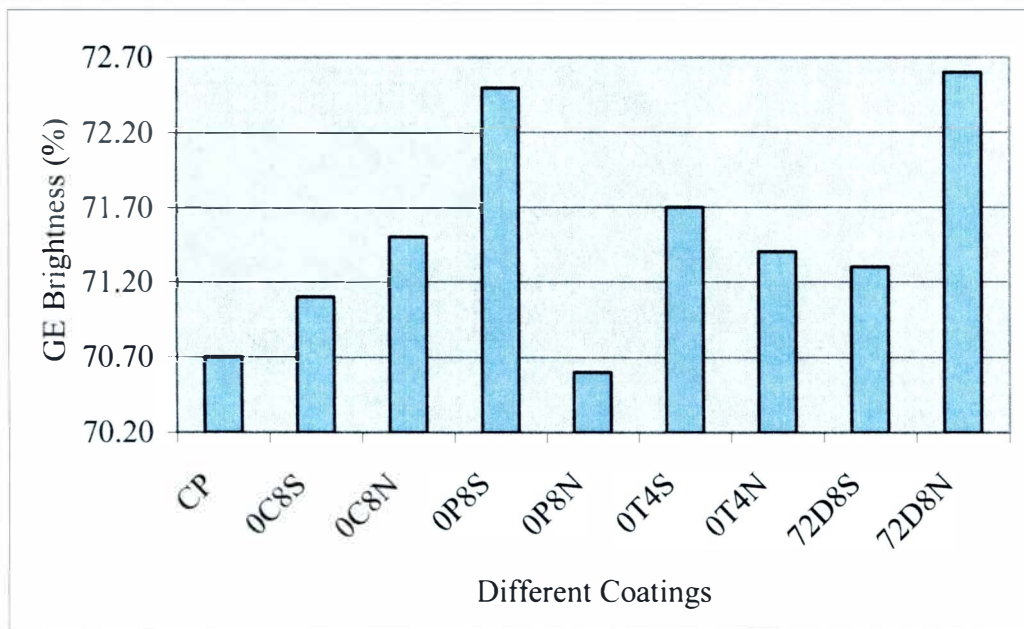
Figure 18. GE Brightness Results as a Function of Different Coatings
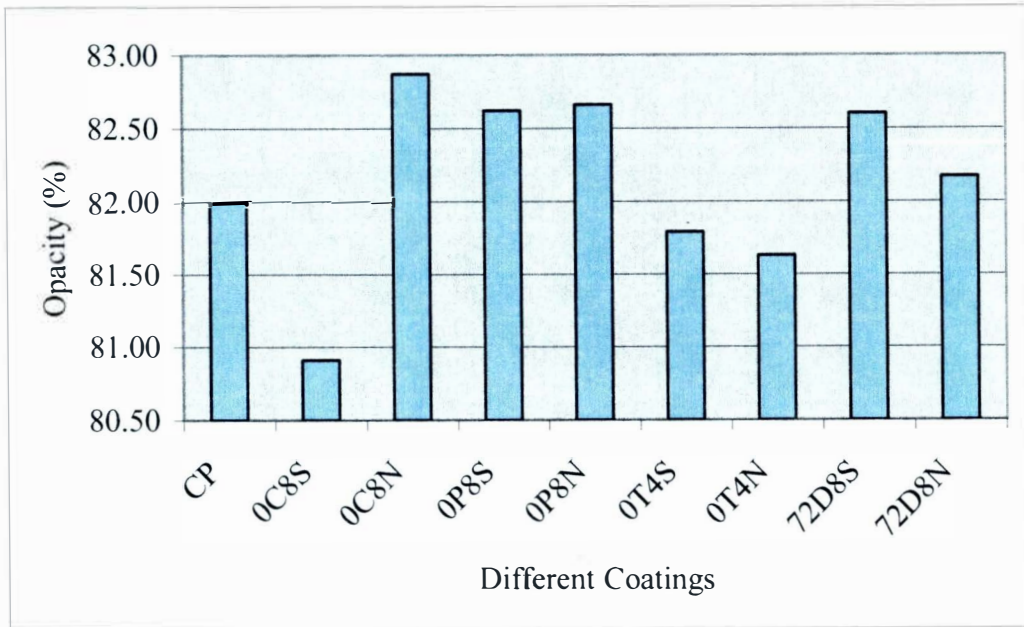
Figure 19. Opacity Results as a Function of Different Coatings
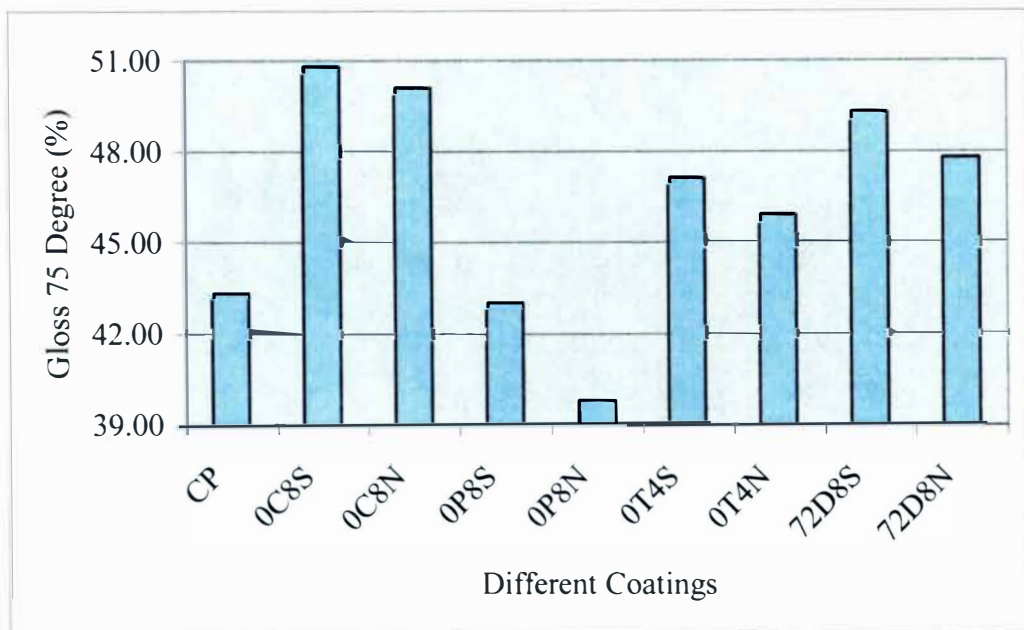
Figure 20. Gloss 75^0 Results as a Function of Different Coatings

Looking at the graphical analysis of confidence level found in Figures 21, 22, and 23 can better compare the differences in the optical properties results. Figure 21 shows the brightness confidence data. The results show that 72D8N and 0P8S gave coatings with the highest brightness. Both the coatings show the same confidence interval. The small confidence interval verifies this as the best brightness results. Figure 22 shows the coated paper opacity confidence data. Coating 0C8N with natural zeolite gave the best opacity followed by coating 0P8N and 0P8S coatings. The small confidence interval for 0C8N & 0P8S verifies this as the best opacity result. However, 0P8N & other coatings had larger confidence intervals that overlap each other. Figure 23 shows the coated paper gloss confidence data. Coating 0C8S with synthetic zeolite gave the best paper gloss followed by coating 0C8N with natural zeolite. However, both the coatings had larger confidence intervals overlapping each other.

Figure 21. GE Brightness Confidence Level as a Function of Different Coatings

Figure 22. Opacity Confidence Level as a Function of Different Coatings
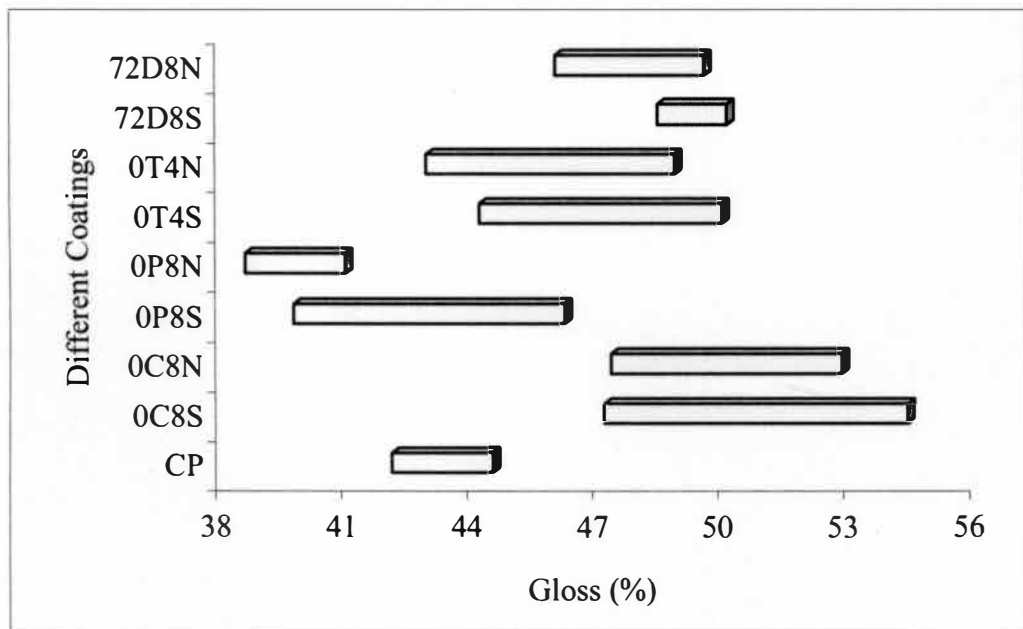
Figure 23. Gloss 75^0 Confidence Level as a Function of Different Coatings

Surface Properties

Table 8 summarizes the surface properties for the control and eight different coatings with zeolite pigments. According to data collected from this experiment, the modified clay zeolite pigment does improve the surface properties, such as PPS smoothness, porosity, and compressibility. LWC papers typically have smoothness values ranging from about 0.90 to 1.1 microns on rotogravure grades.

Table 8

Comparison of Surface Properties of Different Coatings

Coatings	PPS Roughness (μm)		PPS Porosity (ml/min)		Compressibility
	Avg.	STD	Avg.	STD	Avg.
CP	1.03	0.07	1.33	0.07	1.38
0C8S	0.95	0.05	1.40	0.06	1.34
0C8N	0.87	0.02	1.44	0.05	1.35
0P8S	1.08	0.02	1.63	0.07	1.39
0P8N	1.56	0.29	1.93	0.10	1.10
0T4S	0.99	0.03	1.66	0.10	1.27
0T4N	0.99	0.03	1.41	0.03	1.38
72D8S	1.04	0.01	1.79	0.07	1.38
72D8N	1.04	0.05	1.70	0.07	1.35

Figure 24, 25, and 26 show the surface properties tests results. Smoothness is important to control for LWC rotogravure printing because an increase in roughness will increase the number of missing dots. According to the collected data and the graphical analysis of smoothness, coating 0C8N has highest smoothness followed by coating 0C8S. The coating 0P8N has the lowest smoothness. The higher smoothness of the coated surface achieves an increased gloss, better printability, and higher print quality. Figure 25

show the coated paper compressibility results for different coatings. Compressibility is the ratio of PPS roughness at 500 kPa and 1000 kPa. Coating 0P8S has the highest compressibility followed by 0T4N, 72D8S and CP coating. Figure 26 show the coated PPS paper porosity (air permeability) results for different coatings. Coating 0P8N with natural zeolite gave the highest paper porosity. The control coating has the lowest PPS porosity.
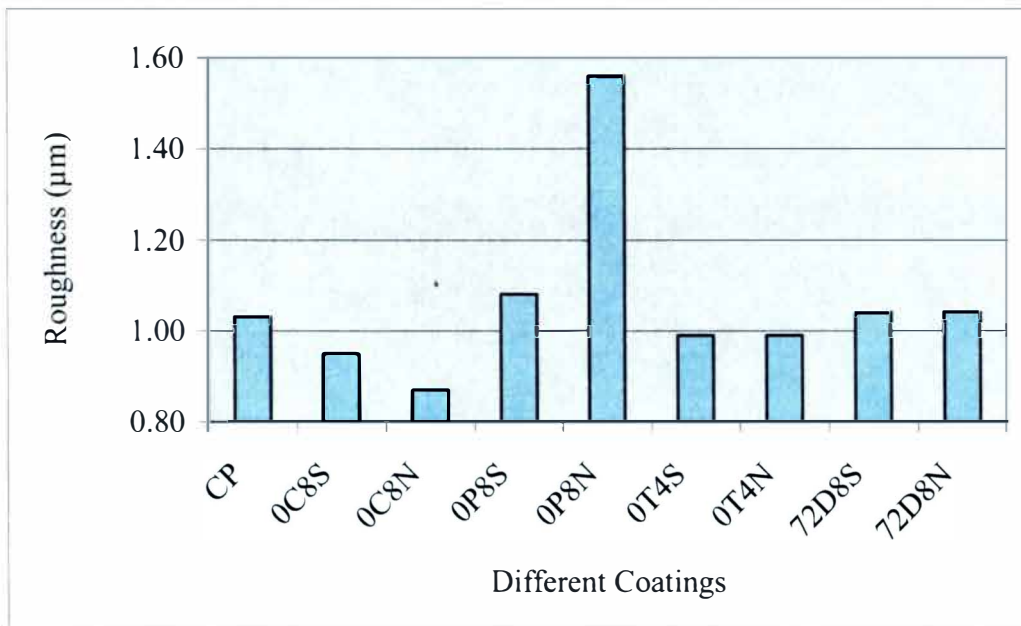
Figure 24. PPS Roughness Results as a Function of Different Coatings
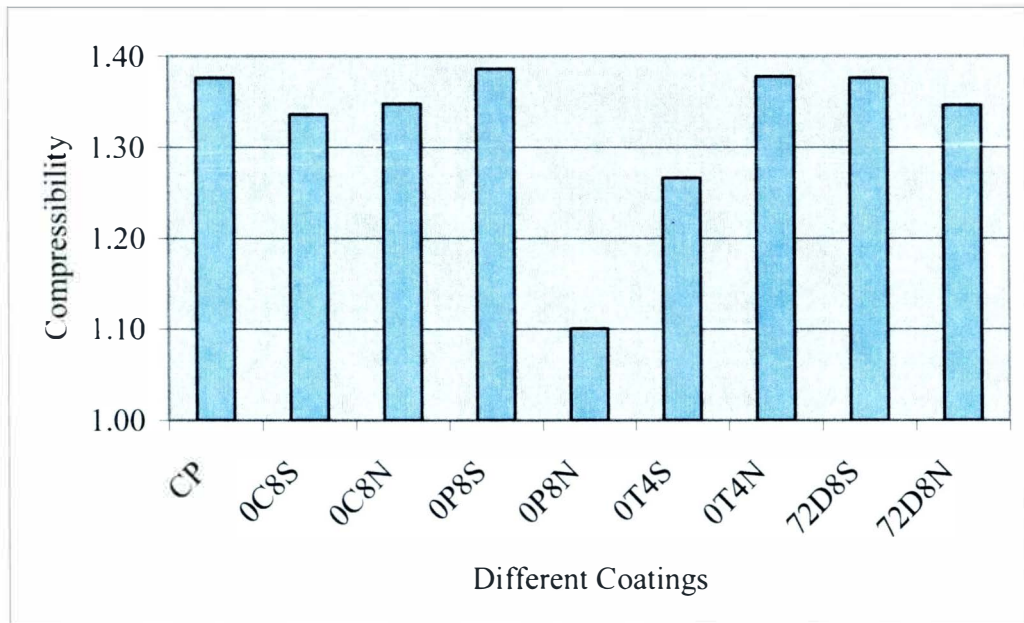
Figure 25. Compressibility Results as a Function of Different Coatings
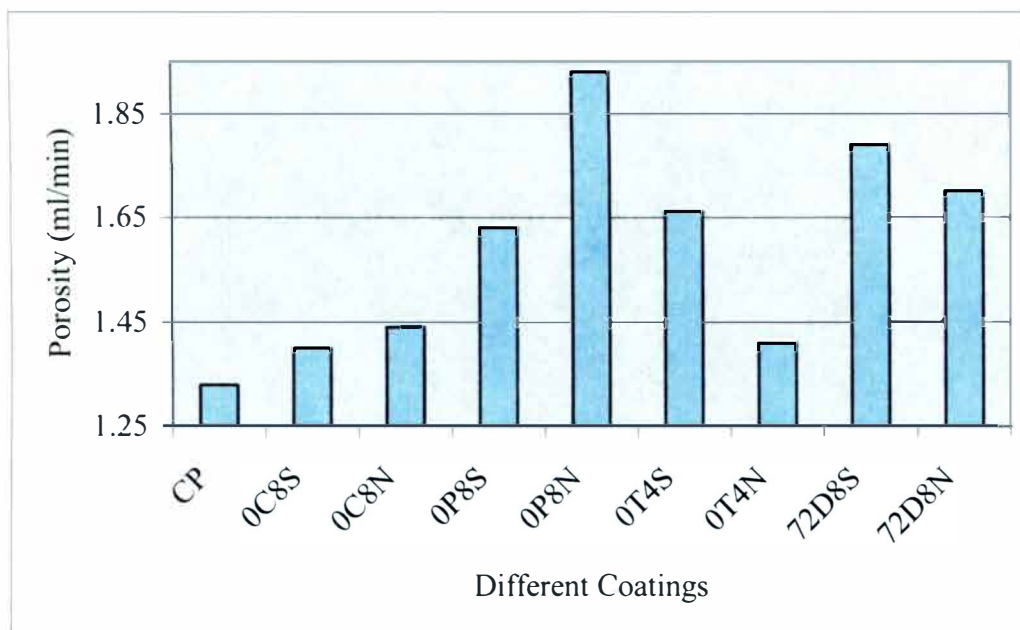
Figure 26. PPS Porosity Results as a Function of Different Coatings

Figure 27 shows the coated paper smoothness confidence data. The lower value of roughness corresponds to a high value of smoothness. Coating 0C8N with natural zeolite gave the best paper smoothness followed by coating 0C8S with synthetic zeolite. The small confidence interval for all the coatings except 0P8N gives a good indication that the number can be trusted. Figure 28 shows the coated paper porosity confidence data. Coating 0P8N with natural zeolite gave the best paper porosity. The control coating has the lowest porosity. All the coating has small confidence interval, which gives a good indication that the numbers can be trusted.
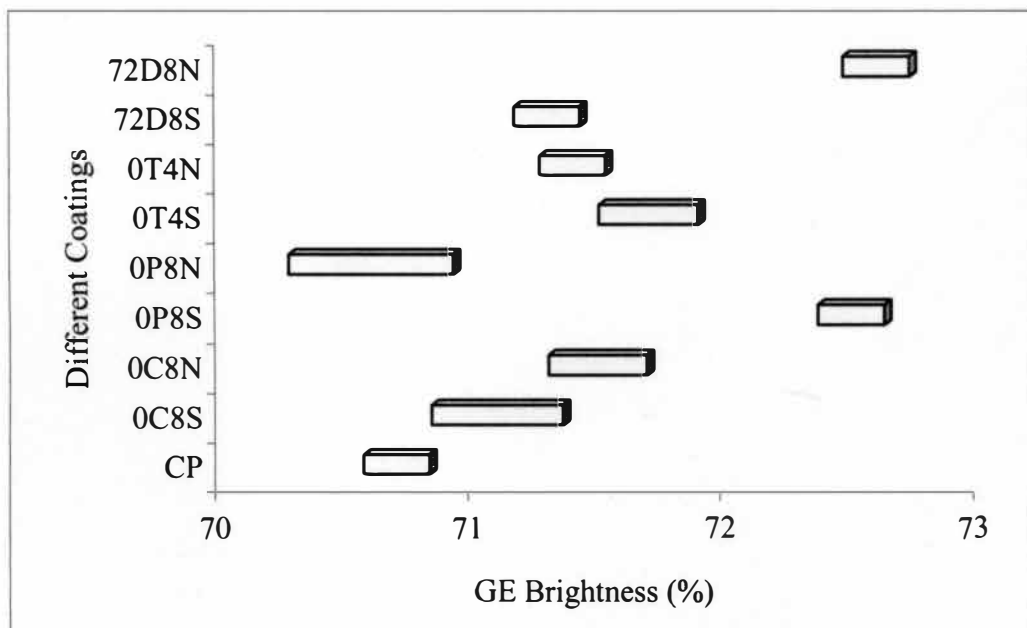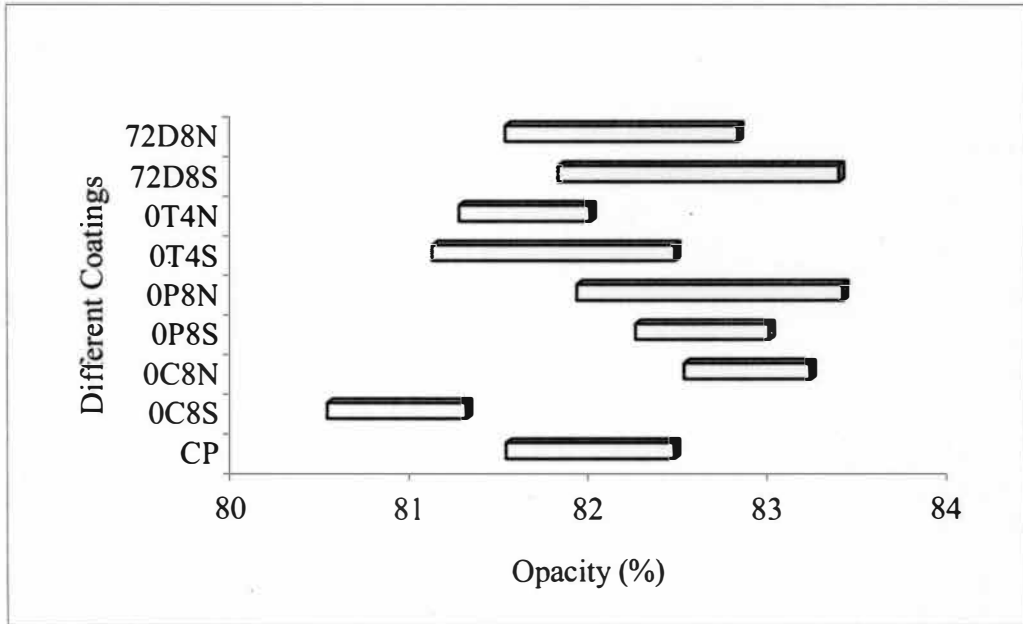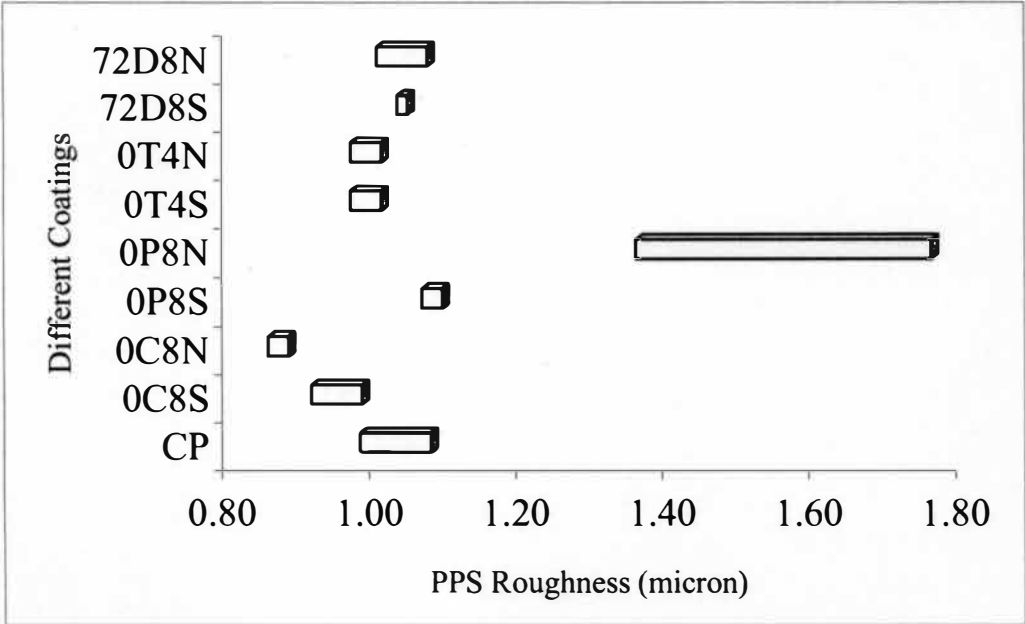

Figure 27. PPS Roughness Confidence Level as a Function of Different Coatings
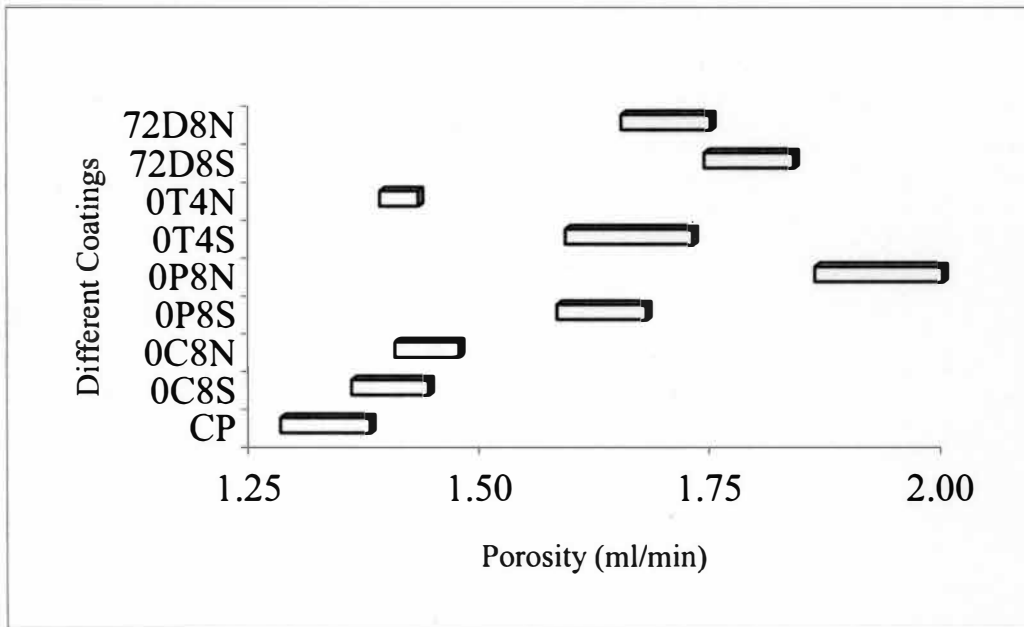
Figure 28. PPS Porosity Confidence Level as a Function of Different Coatings

Print Quality Evaluation

The analysis consisted of a comparison of the control coated samples with zeolite coated sheets on the CLC. All the samples were tested for print density using an x-Rite 408 reflective densitometer. The dot area and roundness are measured using an Image Analyzer. The image analysis software used here is Image Pro Plus. The software and camera are sensitive enough to measure the dot size in microns by counting the screen pixels. The image analyzer was setup to measure the dot area, perimeter and roundness of the printed samples. All the image analysis was performed on the square at the nominal 5 % dot.

Tables 9, 10, and 11 show the image analysis data of different coatings with and without zeolite pigments. The mean and standard deviation with confidence level of dot area, perimeter, and roundness data are included in the Tables below.

Table 9

Image Analysis Dot Area Results of Different Coatings

Coatings	Sum	Mean	STD	% 95 CL	Lower CI	2*CL	Upper CI
CP	582885	3067.8	2003.0	284.8	2783.0	569.6	3352.6
0C8S	560655	2657.2	1505.2	203.1	2454.1	406.2	2860.3
0C8N	612882	3049.2	1756.4	242.8	2806.3	485.6	3292.0
0P8S	609921	2918.3	1570.2	212.9	2705.4	425.8	3131.2
0P8N	539685	2388.0	810.1	105.6	2282.4	211.2	2493.6
0T4S	500463	2394.6	1069.8	145.0	2249.5	290.1	2539.6
0T4N	559467	2742.5	1484.4	203.7	2538.8	407.4	2946.2
72D8S	622620	2882.5	1547.5	206.4	2676.1	412.7	3088.9
72D8N	629622	2956.0	1805.7	242.5	2713.5	485.0	3198.5

Table 10

Image Analysis Dot Perimeter Results of Different Coatings

Coatings	Sum	Mean	STD	% 95 CL	Lower CI	2*CL	Upper CI
CP	58758	309.3	170.1	24.2	285.1	48.4	333.4
0C8S	57779	273.8	137.6	18.6	255.3	37.1	292.4
0C8N	61197	304.5	169.3	23.4	281.1	46.8	327.9
0P8S	61204	292.8	147.4	20.0	272.9	40.0	312.8
0P8N	49680	219.8	56.2	7.3	212.5	14.7	227.2
0T4S	55290	264.5	111.1	15.1	249.5	30.1	279.6
0T4N	66226	324.6	157.7	21.6	303.0	43.3	346.3
72D8S	54850	253.9	114.0	15.2	238.7	30.4	269.1
72D8N	62794	294.8	143.3	19.2	275.6	38.5	314.0

Table 11

Image Analysis Dot Roundness Results of Different Coatings

Coatings	Sum	Mean	STD	% 95 CL	Lower CI	2*CL	Upper CI
CP	512	2.69	1.62	0.23	2.46	0.46	2.92
0C8S	503	2.38	1.33	0.18	2.20	0.36	2.56
0C8N	531	2.64	1.71	0.24	2.41	0.47	2.88
0P8S	523	2.50	1.51	0.21	2.30	0.41	2.71
0P8N	380	1.68	0.50	0.07	1.62	0.13	1.75
0T4S	512	2.45	1.26	0.17	2.28	0.34	2.62
0T4N	676	3.31	1.92	0.26	3.05	0.53	3.58
72D8S	405	1.87	0.87	0.12	1.76	0.23	1.99
72D8N	531	2.49	1.24	0.17	2.33	0.33	2.66

Figure 29 shows the average dot area for water-based ink for coatings with and without zeolite. The coating CP gave the highest ink dot area followed by coating 0C8N. The coating 0P8N and 0T4S showed the lowest ink dot area printed with water-based inks. A high dot area has more spreading (more spreading is not necessarily better, spreading must be enough to fill the solid print, but small enough to produce good highlights, which is desirable for good gravure printing). Figure 32 shows the dot area confidence interval for the different coatings with and without zeolite. All the coatings show longer confidence interval on higher side, hence overlaping. Hence, there is no significant difference in terms of dot area except for 0T4S and 0P8N coatings.

Figure 30 shows the average dot perimeter for water-based ink for coatings with and without zeolite. The coating 0T4N gave highest dot perimeter followed by CP and 0P8N the lowest dot perimeter. The dot perimeter indicates if smear or some spreading mechanism has altered the text quality (the range of allowable perimeter values for that specific character needs to be known). Dot perimeter will increase as the edge becomes more irregular and as the area of the dot increases. Figure 33 shows the dot perimeter confidence interval for the different coatings. Although the confidence intervals are longer, the figure support the above explanation.

Figure 31 shows the average roundness for coated paper printed with water-based inks. The coating 0T4N gave highest dot roundness followed by coating CP and coating 0P8N has the lowest ink dot roundness. Roundness is a measure of circumferential deviation from a circle. Changes in roundness indicate that the dot shape is becoming increasingly irregular over time. Figure 34 shows the dot roundness confidence interval for the different coatings. Again the coatings have longer confidence intervals and overlap. However, the coating 0T4N can easily be seen on the highest and 0P8N on the lowest side.
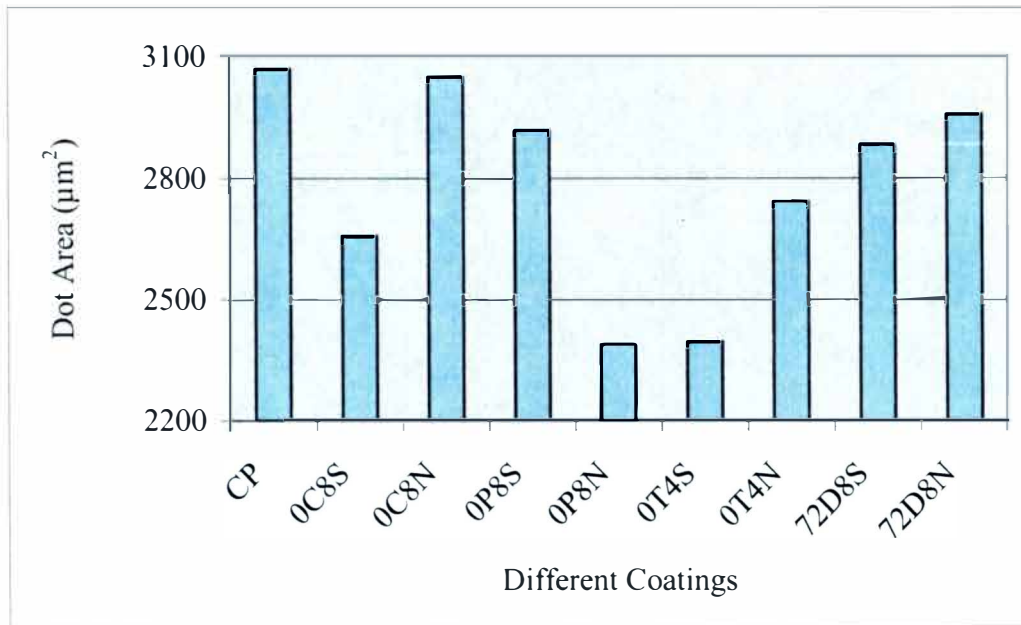
Figure 29. Dot Area Results as a Function of Different Coatings
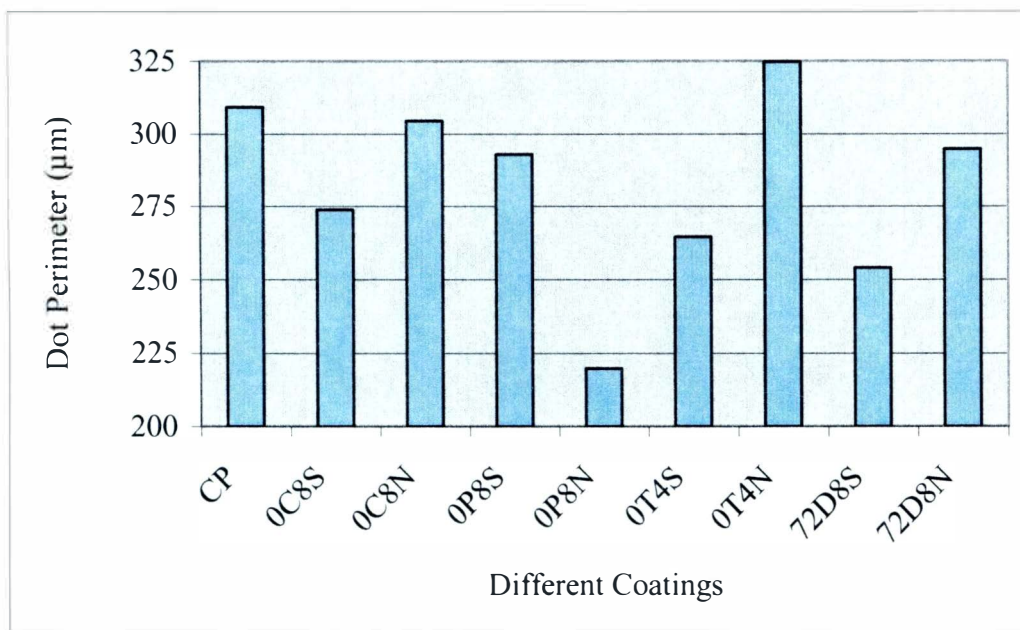
Figure 30. Dot Perimeter Results as a Function of Different Coatings

Figure 31. Dot Roundness Results as a Function of Different Coatings
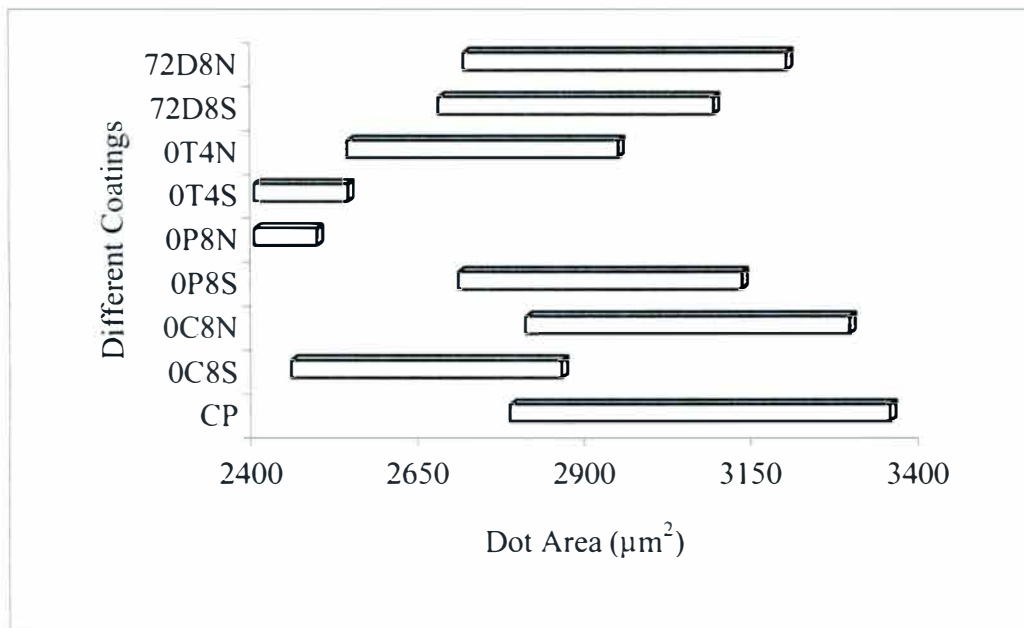
Figure 32. Dot Area Confidence Level as a Function of Different Coatings

Figure 33. Dot Perimeter Confidence Level as a Function of Different Coatings
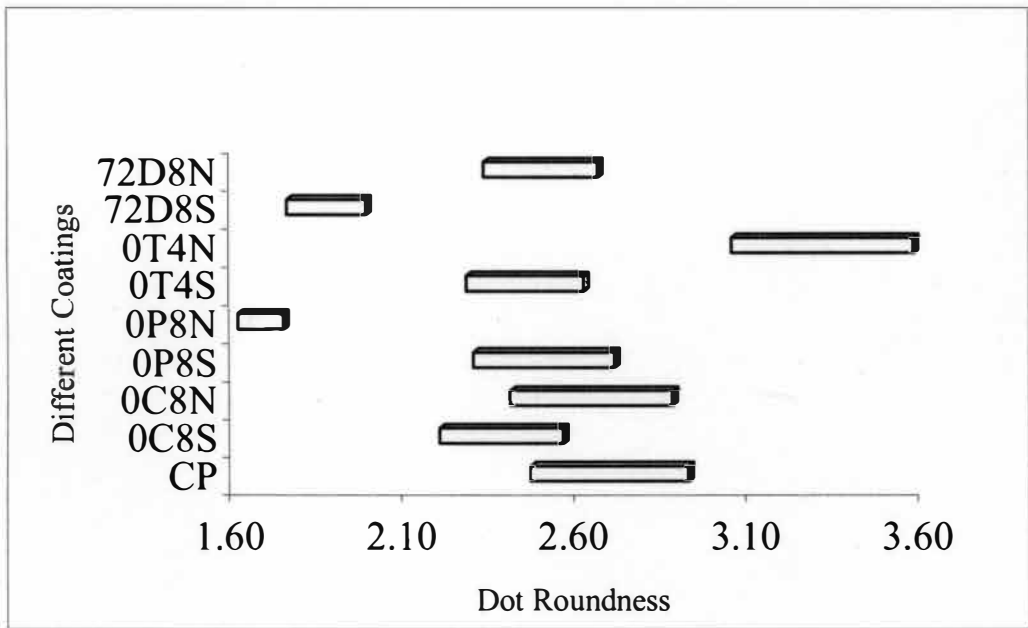
Figure 34. Dot Roundness Confidence Level as a Function of Different Coatings

Optical Density

Table 12 and Figure 35 show the optical density results of different coatings with and without zeolite pigment. The coating 0C8N with natural zeolite showed the highest optical density compared to all other coatings. The coating 0T4S shows second highest optical density followed by 0C8S but has longer confidence interval as can be seen from Figure 36. The coating 0C8S shows smaller confidence interval. Coating 0P8N showed worst optical density. All the coating have small confidence intervals except CP can be distinctly observed.

Table 12

Comparison of Optical Density Results of Different Coatings

Coatings	Avg.	STD	95 % CL	Lower CI	2* CL	Upper CI
CP	1.51	0.10	0.06	1.45	0.12	1.57
0C8S	1.55	0.04	0.02	1.53	0.05	1.57
0C8N	1.63	0.02	0.01	1.61	0.02	1.64
0P8S	1.42	0.03	0.02	1.40	0.04	1.44
0P8N	1.13	0.06	0.04	1.09	0.07	1.17
0T4S	1.57	0.06	0.04	1.53	0.07	1.60
0T4N	1.55	0.01	0.01	1.54	0.02	1.56
72D8S	1.50	0.03	0.02	1.49	0.03	1.52
72D8N	1.49	0.04	0.02	1.47	0.04	1.52
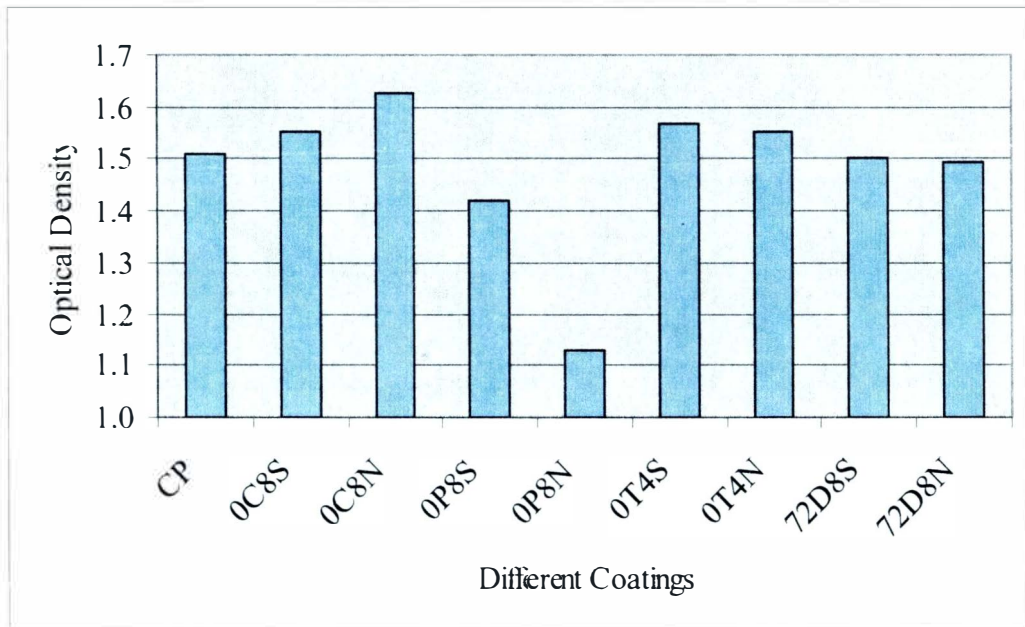
Figure 35. Optical Density Results as a Function of Different Coatings
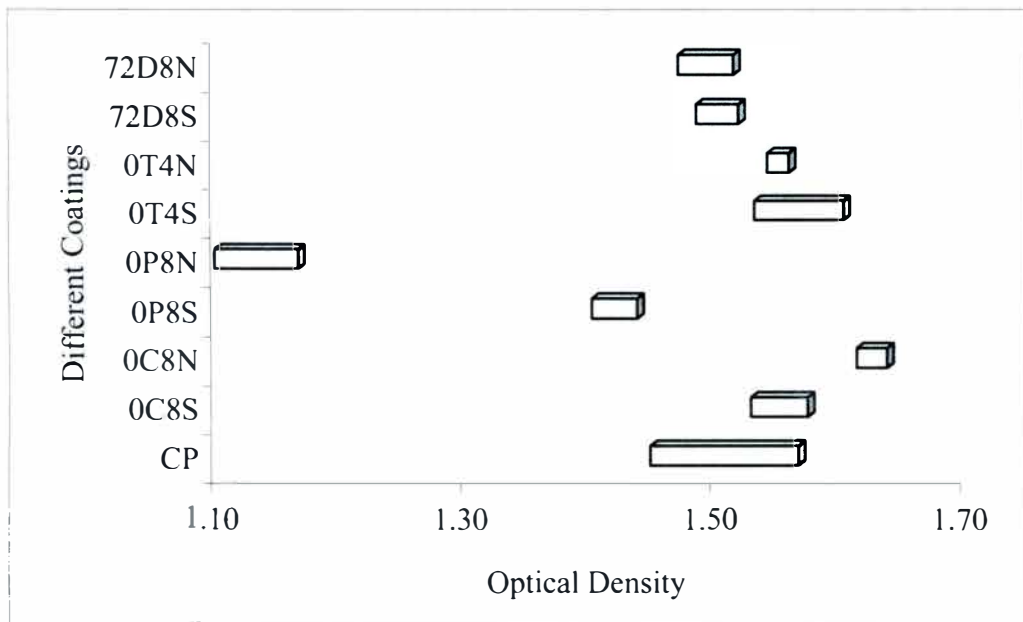
Figure 36. Optical Density Confidence Level as a Function of Different Coatings

Print Gloss

Table 13 represents the paper and print gloss results measured at 60 degree angle. The table also shows the delta gloss results, the difference of print gloss and paper gloss at 60 degree. Figure 37 and 38 show the print gloss and delta gloss for different coatings with and without zeolite pigment. The coating 0T4S with synthetic zeolite showed the highest print gloss followed by 0C8N compared to all other coatings with and without zeolite. The coating 0P8S with synthetic zeolite gave the highest delta gloss followed by 72D8N. The Figure 39 shows the print gloss confidence data. Again coating 0P8N showed the worst print gloss over the other coating. All the coating have smaller confidence intervals and can be distinctly observed.

Table 13

Comparison of Print, Paper and Delta Gloss Results of Different Coatings

| Coatings	Print Gloss 60^0		Paper Gloss 60^0		Delta Gloss
	Avg.	STD	Avg.	STD	Avg.
CP	14.82	1.01	12.06	0.75	2.76
0C8S	14.97	0.75	11.55	0.72	3.42
0C8N	17.22	1.80	14.64	1.13	2.58
0P8S	15.30	1.55	10.31	1.60	4.99
0P8N	8.78	0.98	6.05	0.92	2.73
0T4S	18.46	2.94	14.81	1.75	3.65
0T4N	16.59	1.65	13.03	0.61	3.56
72D8S	16.80	1.34	13.14	1.05	3.66
72D8N	13.84	1.05	9.22	0.96	4.62
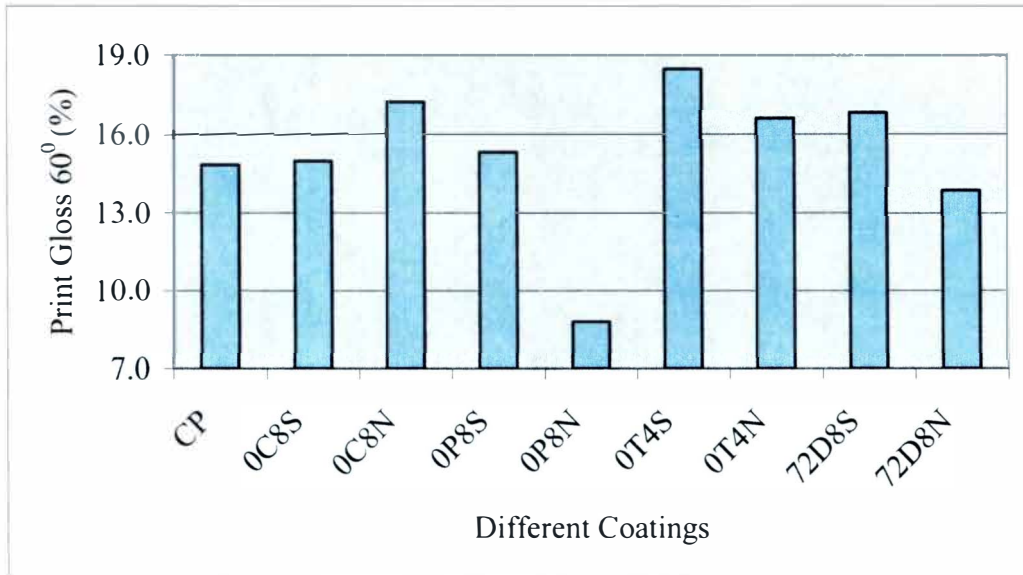
Figure 37. Print Gloss 60^0 Results as a Function of Different Coatings
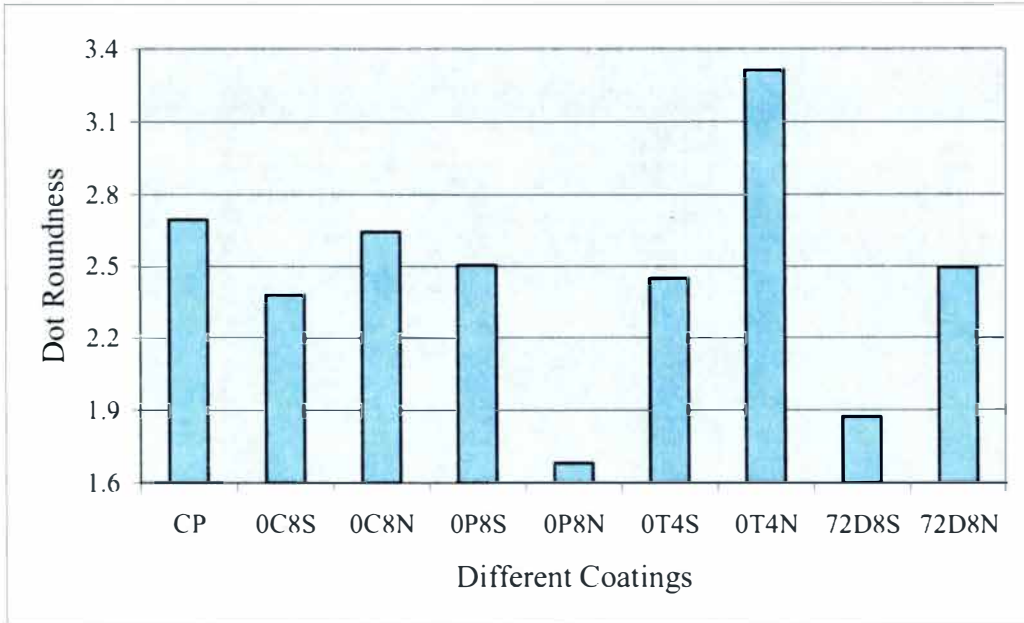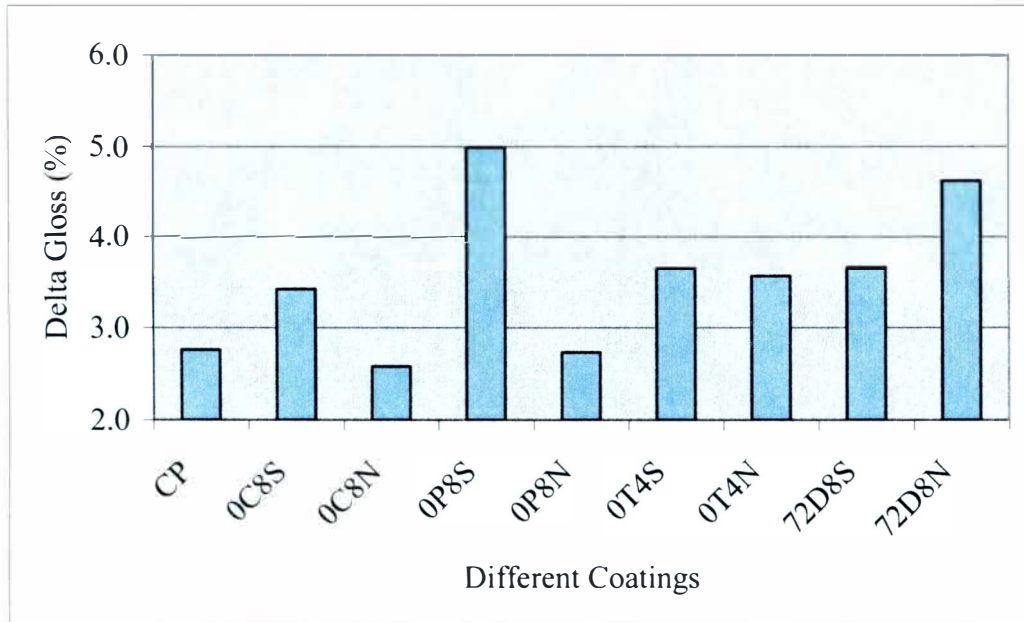

Figure 38. Delta Gloss Results as a Function of Different Coatings

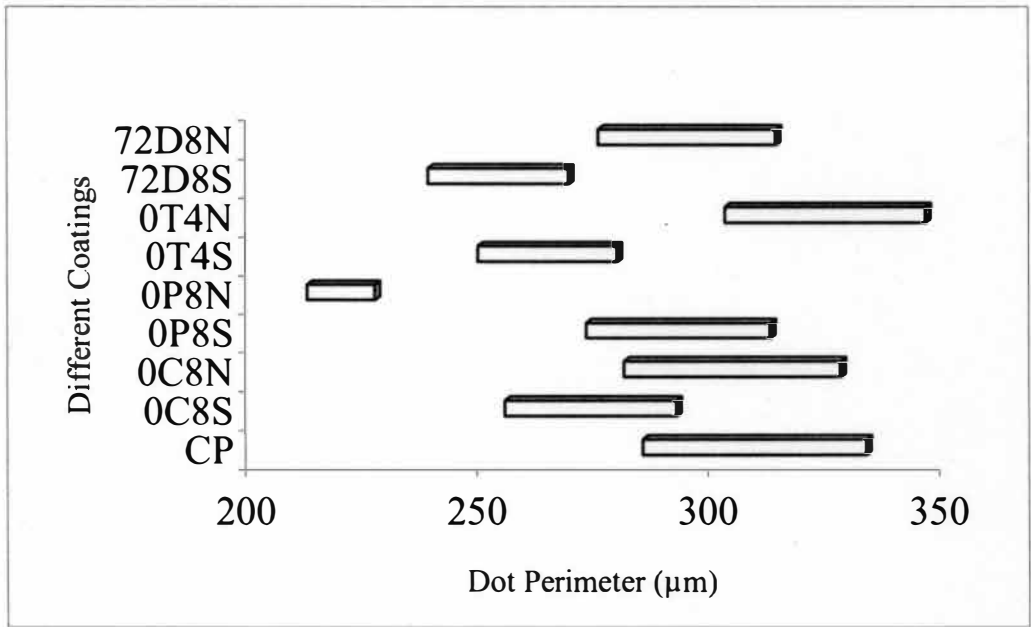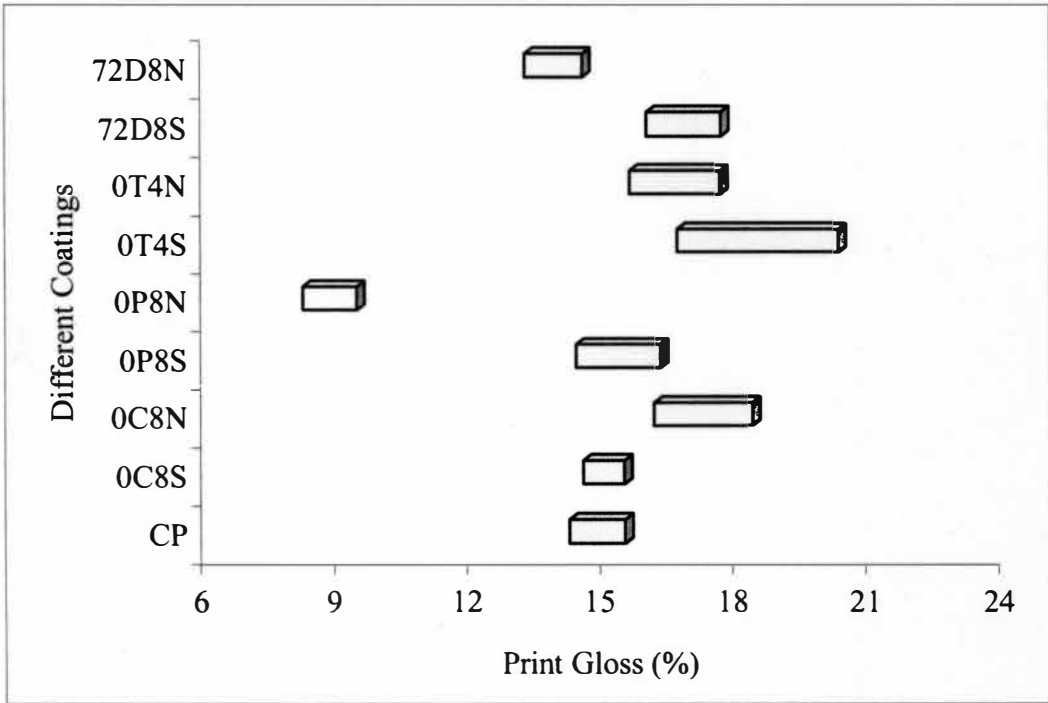Figure 39. Print Gloss Confidence Level as a Function of Different Coatings

CHAPTER VI

CONCLUSIONS

The research investigated the application of modified clay zeolite pigment in matte coated LWC formulations for rotogravure. The rheological, structural, optical, surface and print properties of the coatings were compared to the control coated sheets. From this research, it can be concluded that:

- The modified clay zeolite showed promising results as a pigment in the LWC rotogravure formulations.

- TriStar™ 3000 nitrogen gas adsorption very clearly shows that porous zeolite pigment has the highest micropore area, external area, and BET surface area.

- All the coatings were found to be viscoelastic under conditions tested. The storage modulus (G') was higher than the loss modulus (G"), indicating the network structures.

- The natural zeolite coatings gave the lowest contact angle compared to control and synthetic zeolite measured with deionized water.

- The natural zeolite coatings gave faster liquid penetration compared to control and synthetic zeolite.

- All the coatings except 0P8N gave higher brightness compared to control coating.

- All the coatings except 0C8S, 0T4S and 0T4N gave higher opacity compared to control coating.

- All the coatings except 0P8S, 0P8N gave higher paper gloss compared to control coating.

- All the coatings except 0P8N gave comparable PPS roughness to the control coating.

- All the coatings gave higher PPS porosity compared to control coating.

- All the coatings gave lower dot area compared to control coating.

- All the coatings except 0T4N gave lower dot perimeter and roundness compared to control coating.

- All the coatings 0P8N gave comparable optical density to control coating.

- All the coatings except 0P8N, 72D8N gave higher print gloss compared to control coating.

CHAPTER VI

SUGGESTIONS FOR FURTHER STUDY

- Higher amount of zeolite pigment could be used to see how different coating properties varied.

- Additional studies are required to better understand the influence of porous zeolite on print quality. This includes the optimization of printing condition such as speed and nip load because of variation due to backing web, which will assist in predicting the print quality accurately.

- It would also be helpful to test the commercial LWC sheet for this research to better correlate the print quality.

- Different color water-based inks could be used to see how different inks interact with the zeolite containing coating surfaces.

APPENDICES

Appendix A

Operating Conditions for the CLC

The CLC (cylindrical laboratory coater)-6000 can apply coatings at surface speeds up to 6000 fpm (1900 m/min). In this study a coating speed of 3000 fpm was used. The CLC conditions used for this study are listed in Table 14. The CLC consists of a rotating Backing Roll, with a diameter of 40 inches (1016 mm), where the paper is mounted on. A Pond which can hold a coating up to one gallon. The Pond is placed on a carriage which moves across the surface of the backing roll to apply the coating volume onto the paper during the coating process. A Control Panel controls the roll speed, blade pressure, and drying temperature. The CLC utilizes infrared heat, applied in a unique manner that insures that every square inch of coated surface receives the same drying treatment.

Table 14

CLC Operating Conditions

Operating Speed (fpm)	3000
Coating Blade Extension (in.)	1.20
Coating Blade Thickness (in.)	0.025
Backing Blade Thickness (in.)	0.025
Backing Blade Free Extension (in.)	0.4-0.5
Pre Drying (secs/%)	10-15/15
Post Drying (secs/%)	40-50/100
Pond Angle (degrees)	50
Drying Delay Distance (meters)	5

Appendix B

Supporting Data

Table 15

Average Dynamic Contact Angle Results of Different Coatings

Coatings	CP	0C8S	0C8N	0P8S	0P8N	0T4S	0T4N	72D8S	72D8N
1	58.75	70.34	56.17	63.83	36.75	72.26	63.37	61.20	59.75
2	59.08	69.02	57.11	63.07	35.45	72.85	57.64	64.41	53.44
3	63.88	67.05	59.85	63.37	37.81	67.52	57.36	67.76	52.46
4	59.84	70.07	60.53	63.01	37.02	68.00	60.63	69.21	57.90
5	58.05	68.77	59.97	60.91	37.11	60.18	57.69	66.31	51.45
Avg.	59.92	69.05	58.73	62.84	36.83	68.16	59.34	65.78	55.00
STD	2.31	1.30	1.95	1.13	0.86	5.07	2.62	3.12	3.62
95 % CL	1.43	0.81	1.21	0.70	0.54	3.14	1.62	1.93	2.24
Lower CI	58.49	68.24	57.52	62.14	36.29	65.02	57.71	63.85	52.76
2* CL	2.86	1.61	2.42	1.40	1.07	6.29	3.25	3.86	4.49
Upper CI	61.35	69.86	59.93	63.54	37.36	71.31	60.96	67.71	57.24

Table 16

GE Brightness Confidence Level Results of Different Coatings

Coatings	Avg.	STD	95% CL	Lower CI	2* CL	Upper CI
CP	70.70	0.20	0.13	70.57	0.26	70.83
0C8S	71.10	0.40	0.26	70.84	0.52	71.36
0C8N	71.50	0.30	0.20	71.30	0.39	71.70
0P8S	72.50	0.20	0.13	72.37	0.26	72.63
0P8N	70.60	0.50	0.33	70.27	0.65	70.93
0T4S	71.70	0.30	0.20	71.50	0.39	71.90
0T4N	71.40	0.20	0.13	71.27	0.26	71.53
72D8S	71.30	0.20	0.13	71.17	0.26	71.43
72D8N	72.60	0.20	0.13	72.47	0.26	72.73

Table 17

Opacity Confidence Level Results of Different Coatings

Coatings	Avg.	STD	95% CL	Lower CI	2* CL	Upper CI
CP	81.99	0.68	0.47	81.52	0.94	82.46
0C8S	80.91	0.56	0.39	80.52	0.78	81.30
0C8N	82.87	0.51	0.35	82.52	0.71	83.22
0P8S	82.62	0.54	0.37	82.25	0.75	82.99
0P8N	82.66	1.07	0.74	81.92	1.48	83.40
0T4S	81.79	0.98	0.68	81.11	1.36	82.47
0T4N	81.63	0.53	0.37	81.26	0.73	82.00
72D8S	82.60	1.13	0.78	81.82	1.57	83.38
72D8N	82.17	0.94	0.65	81.52	1.30	82.82

Table 18

Gloss 75^0 Confidence Level Results of Different Coatings

Coatings	Avg.	STD	95% CL	Lower CI	2* CL	Upper CI
CP	43.30	1.74	1.21	42.09	2.41	44.51
0C8S	50.80	5.22	3.62	47.18	7.23	54.42
0C8N	50.10	3.98	2.76	47.34	5.52	52.86
0P8S	43.00	4.68	3.24	39.76	6.49	46.24
0P8N	39.80	1.73	1.20	38.60	2.40	41.00
0T4S	47.10	4.20	2.91	44.19	5.82	50.01
0T4N	45.90	4.30	2.98	42.92	5.96	48.88
72D8S	49.30	1.19	0.82	48.48	1.65	50.12
72D8N	47.80	2.58	1.79	46.01	3.58	49.59

Table 19

PPS Roughness Confidence Level Results of Different Coatings

Coatings	Avg.	STD	95% CL	Lower CI	2* CL	Upper CI
CP	1.03	0.07	0.05	0.98	0.10	1.08
0C8S	0.95	0.05	0.03	0.92	0.07	0.98
0C8N	0.87	0.02	0.01	0.86	0.03	0.88
0P8S	1.08	0.02	0.01	1.07	0.03	1.09
0P8N	1.56	0.29	0.20	1.36	0.40	1.76
0T4S	0.99	0.03	0.02	0.97	0.04	1.01
0T4N	0.99	0.03	0.02	0.97	0.04	1.01
72D8S	1.04	0.01	0.01	1.03	0.01	1.05
72D8N	1.04	0.05	0.03	1.01	0.07	1.07

Table 20

PPS Porosity Confidence Level Results of Different Coatings

Coatings	Avg.	STD	95% CL	Lower CI	2* CL	Upper CI
CP	1.33	0.07	0.05	1.28	0.10	1.38
0C8S	1.40	0.06	0.04	1.36	0.08	1.44
0C8N	1.44	0.05	0.03	1.41	0.07	1.47
0P8S	1.63	0.07	0.05	1.58	0.10	1.68
0P8N	1.93	0.10	0.07	1.86	0.14	2.00
0T4S	1.66	0.10	0.07	1.59	0.14	1.73
0T4N	1.41	0.03	0.02	1.39	0.04	1.43
72D8S	1.79	0.07	0.05	1.74	0.10	1.84
72D8N	1.70	0.07	0.05	1.65	0.10	1.75

Table 21

Image Analysis Results of Different Coatings

Control Coating CP					
Stats	Area	Perimeter	Roundness	Fractal Dim.	Dendrites
Min	52	35.44	1.04	1.06	0
(Obj.#)	158	70	70	445	8
Max	2237	551.70	10.83	1.34	5
(Obj.#)	108	108	108	108	77
Range	2185	516.26	9.79	0.29	5
Mean	3067.82	309.25	2.69	1.14	0.65
Std.Dev	2002.97	170.13	1.62	0.05	0.90
Sum	582885	58758.15	511.94	217.23	123
Samples	190	190	190	190	190

Coating 0C8S					
Stats	Area	Perimeter	Roundness	Fractal Dim.	Dendrites
Min	59	33.95	1	1.049	0
(Obj.#)	368	368	339	167	8
Max	1640	377.06	9.01	1.33	3
(Obj.#)	265	265	79	185	41
Range	1581	343.11	8.01	0.28	3
Mean	2657.16	273.84	2.38	1.13	0.52
Std.Dev	1505.16	137.55	1.33	0.044	0.73
Sum	560655	57779.43	502.80	237.41	108
Samples	211	211	211	211	211

Coating 0C8N					
Stats	Area	Perimeter	Roundness	Fractal Dim.	Dendrites
Min	52	33.30	1	1.051	0
(Obj.#)	121	9	65	164	9
Max	1590	483.05	11.68	1.29	4
(Obj.#)	46	46	46	46	108
Range	1538	449.76	10.69	0.24	4
Mean	3049.1642	304.46	2.64	1.13	0.55
Std.Dev	1756.4395	169.27	1.71	0.050	0.74
Sum	612882	61196.59	531.20	227.62	111
Samples	201	201	201	201	201

Coating 0P8S					
Stats	Area	Perimeter	Roundness	Fractal Dim.	Dendrites
Min	61	31.65	1	1.06	0
(Obj.#)	403	403	71	21	3
Max	1546	465.49	11.86	1.33	4
(Obj.#)	311	311	151	151	244
Range	1485	433.84	10.86	0.27	4
Mean	2918.28	292.84	2.50	1.13	0.56
Std.Dev	1570.20	147.37	1.51	0.04	0.82
Sum	609921.00	61203.90	523.43	236.88	117
Samples	209	209	209	209	209

Coating 0P8N					
Stats	Area	Perimeter	Roundness	Fractal Dim.	Dendrites
Min	54	32.27	1	1.04	0
(Obj.#)	94	315	33	200	2
Max	714	173.58	3.68	1.32	4
(Obj.#)	206	183	183	315	79
Range	660	141.32	2.68	0.28	4
Mean	2387.98	219.82	1.68	1.12	0.30
Std.Dev	810.14	56.23	0.50	0.04	0.57
Sum	539685	49680.22	380.01	253.65	67
Samples	226	226	226	226	226

Coating 0T4S					
Stats	Area	Perimeter	Roundness	Fractal Dim.	Dendrites
Min	57	29.79	1	1.04	0
(Obj.#)	362	52	52	94	16
Max	729	259.18	8.87	1.38	4
(Obj.#)	146	65	286	17	377
Range	672	229.39	7.87	0.34	4
Mean	2394.56	264.55	2.45	1.13	0.52
Std.Dev	1069.79	111.09	1.26	0.04	0.69
Sum	500463	55290.27	511.94	236.60	108
Samples	209	209	209	209	209

Coating 0T4N					
Stats	Area	Perimeter	Roundness	Fractal Dim.	Dendrites
Min	49	33.61	1	1.06	0
(Obj.#)	193	433	371	111	13
Max	1247	335.29	11.14	1.29	6
(Obj.#)	363	310	392	176	392
Range	1198	301.68	10.14	0.23	6
Mean	2742.48	324.64	3.31	1.15	0.56
Std.Dev	1484.44	157.72	1.92	0.05	0.93
Sum	559467	66225.77	675.78	234.56	115
Samples	204	204	204	204	204

Coating 72D8S					
Stats	Area	Perimeter	Roundness	Fractal Dim.	Dendrites
Min	66	30.39	1	1.06	0
(Obj.#)	177	221	36	368	10
Max	1411	298.54	5.74	1.28	7
(Obj.#)	85	85	163	299	85
Range	1345	268.15	4.74	0.22	7
Mean	2882.50	253.94	1.87	1.12	0.63
Std.Dev	1547.45	114.03	0.87	0.04	1.09
Sum	622620	54850.34	404.59	242.33	135
Samples	216	216	216	216	216

Coating 72D8N					
Stats	Area	Perimeter	Roundness	Fractal Dim.	Dendrites
Min	61	32.16	1.01	1.07	0
(Obj.#)	347	347	21	143	5
Max	1682	376.35	7.83	1.30	3
(Obj.#)	372	372	162	84	28
Range	1621	344.19	6.82	0.23	3
Mean	2955.97	294.80	2.49	1.14	0.52
Std.Dev	1805.74	143.26	1.24	0.05	0.80
Sum	629622	62794.49	531.41	242.84	111
Samples	213	213	213	213	213

Table 22

Optical Density Results of Different Coatings

Coatings	CP	0C8S	0C8N	0P8S	0P8N	0T4S	0T4N	72D8S	72D8N
1	1.48	1.58	1.59	1.44	1.10	1.52	1.54	1.52	1.50
2	1.48	1.50	1.60	1.41	1.06	1.52	1.53	1.48	1.51
3	1.40	1.50	1.62	1.41	1.21	1.51	1.57	1.48	1.50
4	1.38	1.52	1.63	1.41	1.17	1.53	1.54	1.47	1.52
5	1.38	1.53	1.62	1.44	1.07	1.58	1.54	1.49	1.47
6	1.59	1.56	1.63	1.41	1.05	1.65	1.56	1.48	1.44
7	1.57	1.57	1.64	1.39	1.20	1.65	1.56	1.51	1.43
8	1.61	1.57	1.65	1.37	1.17	1.64	1.55	1.55	1.52
9	1.58	1.59	1.63	1.46	1.15	1.55	1.55	1.53	1.52
10	1.61	1.60	1.65	1.46	1.12	1.53	1.57	1.52	1.53
Avg.	1.508	1.552	1.626	1.420	1.130	1.568	1.551	1.503	1.494
STD	0.096	0.037	0.020	0.029	0.058	0.058	0.014	0.027	0.035
95 % CL	0.06	0.02	0.01	0.02	0.04	0.04	0.01	0.02	0.02
Lower CI	1.45	1.53	1.61	1.40	1.09	1.53	1.54	1.49	1.47
2* CL	0.12	0.05	0.02	0.04	0.07	0.07	0.02	0.03	0.04
Upper CI	1.57	1.57	1.64	1.44	1.17	1.60	1.56	1.52	1.52

Table 23

Print Gloss 60^0 Results of Different Coatings

| Coatings	CP	0C8S	0C8N	0P8S	0P8N	0T4S	0T4N	72D8S	72D8N
1	15.20	15.10	16.40	15.60	8.60	14.30	17.30	18.00	14.30
2	14.50	15.80	16.90	16.30	9.10	13.20	18.50	17.70	14.10
3	15.20	15.40	18.90	17.90	10.00	16.90	18.40	18.00	14.40
4	15.00	13.90	18.60	17.30	10.50	18.70	16.30	17.90	15.20
5	15.20	15.50	18.30	13.40	9.50	19.00	16.60	16.70	14.70
6	14.50	14.40	19.10	13.10	7.50	19.70	14.80	18.20	13.20
7	12.20	13.60	18.50	14.30	8.50	21.80	14.30	15.60	12.80
8	15.90	15.60	16.50	14.90	8.40	21.60	14.20	14.70	11.60
9	15.00	15.10	13.50	15.00	7.80	21.20	17.40	15.10	14.30
10	15.50	15.30	15.50	15.20	7.90	18.20	18.10	16.10	13.80
Avg.	14.82	14.97	17.22	15.30	8.78	18.46	16.59	16.80	13.84
STD	1.01	0.75	1.80	1.55	0.98	2.94	1.65	1.34	1.05
95 % CL	0.63	0.46	1.12	0.96	0.61	1.82	1.02	0.83	0.65
Lower CI	14.19	14.51	16.10	14.34	8.17	16.64	15.57	15.97	13.19
2* CL	1.25	0.93	2.23	1.92	1.22	3.65	2.05	1.66	1.30
Upper CI	15.45	15.43	18.34	16.26	9.39	20.28	17.61	17.63	14.49

Appendix C

Printing Images
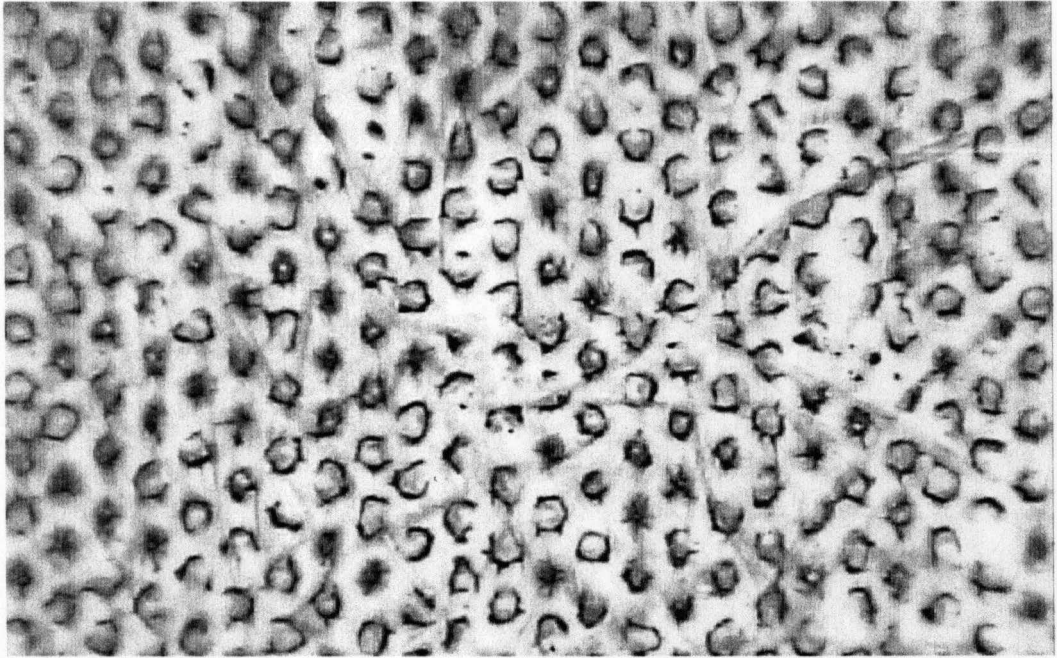
Figure 40. Printing Image of CP Coated Paper Printed With Water-Based Ink
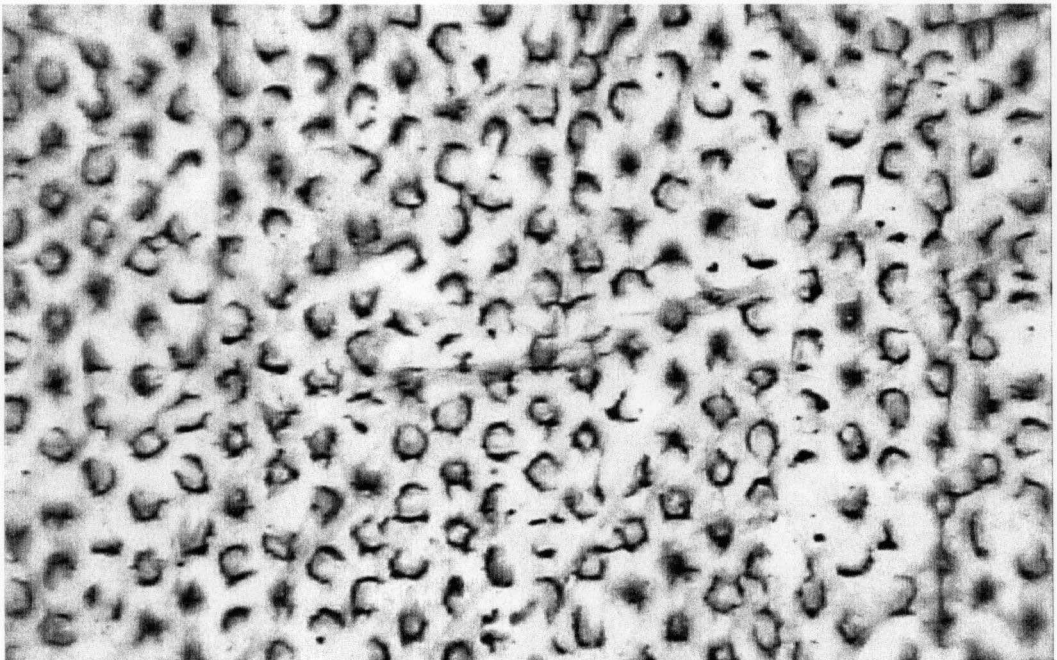

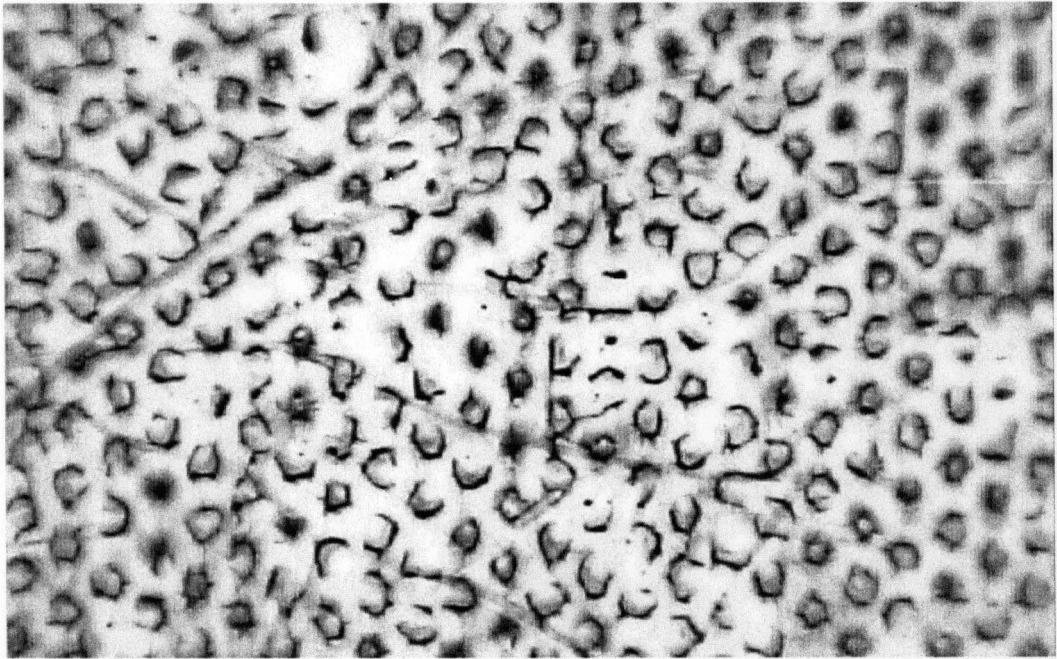Figure 41. Printing Image of 0C8S Coated Paper Printed With Water-Based Ink

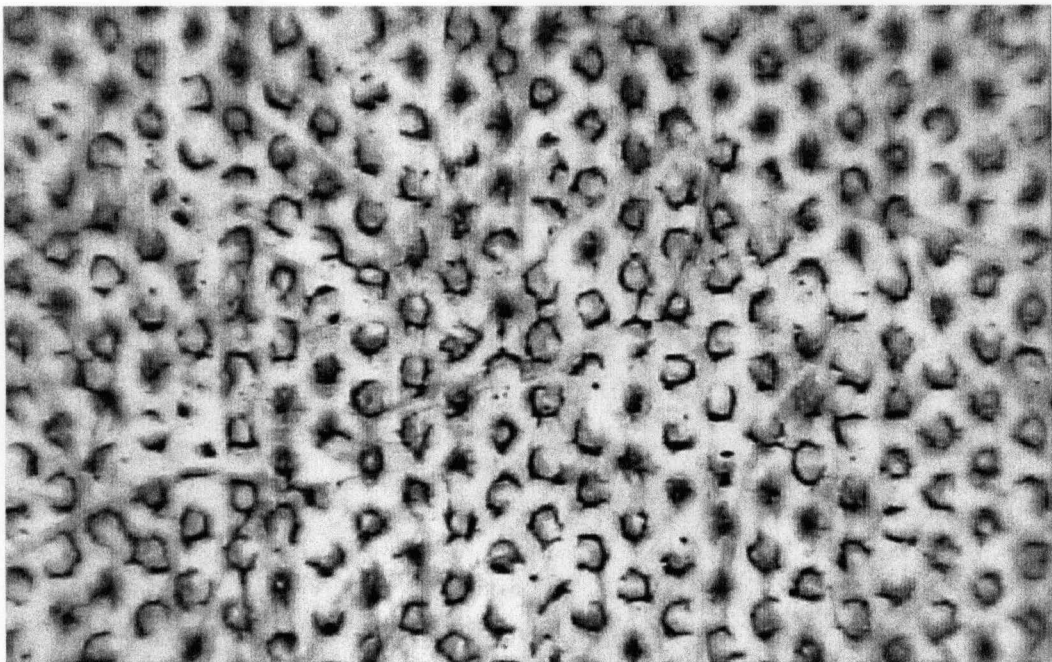Figure 42. Printing Image of 0C8N Coated Paper Printed With Water-Based Ink

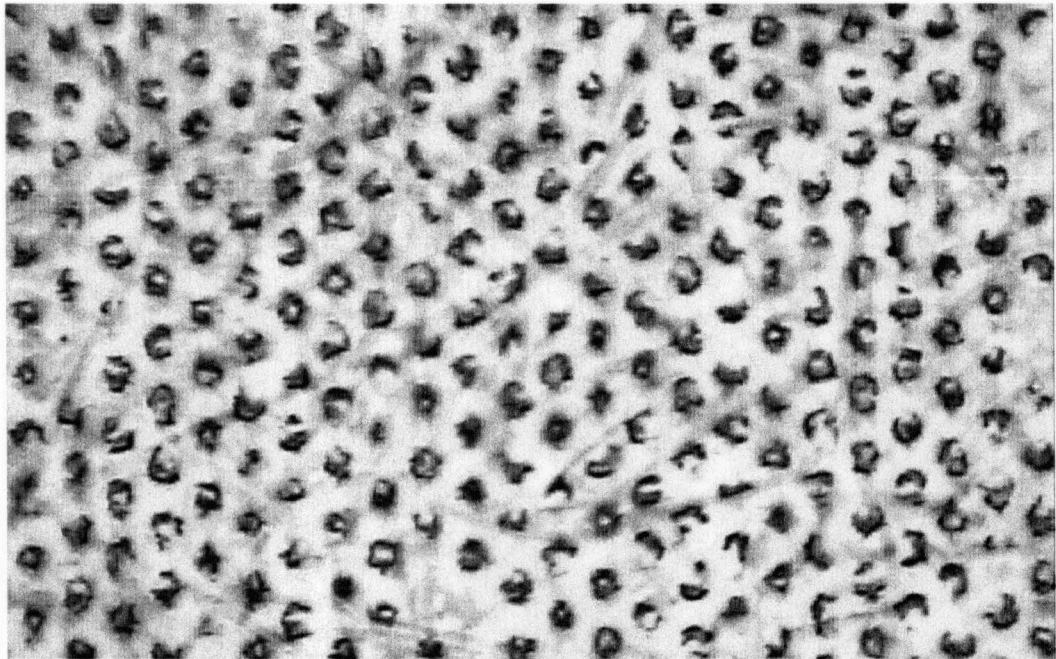Figure 43. Printing Image of 0P8S Coated Paper Printed With Water-Based Ink

Figure 44. Printing Image of 0P8N Coated Paper Printed With Water-Based Ink
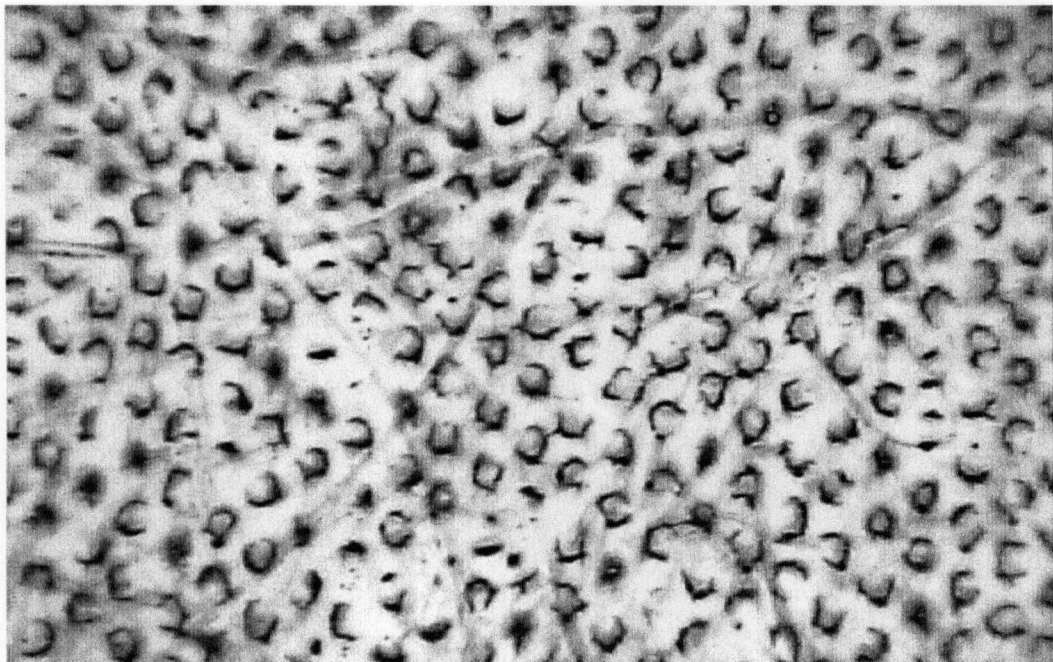

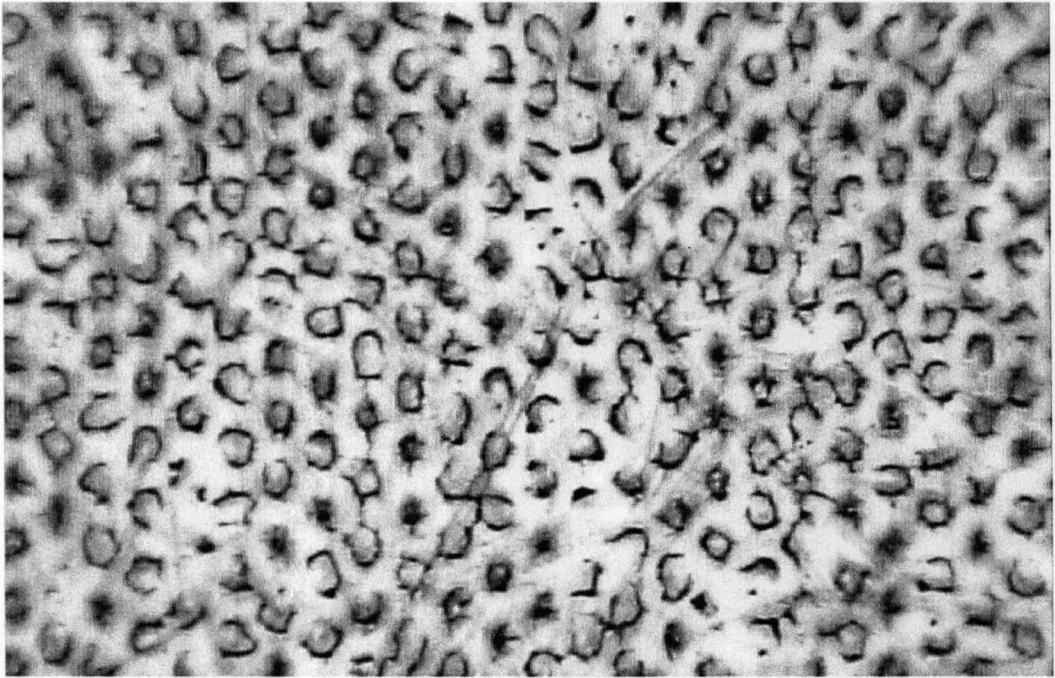Figure 45. Printing Image of 0T4S Coated Paper Printed With Water-Based Ink

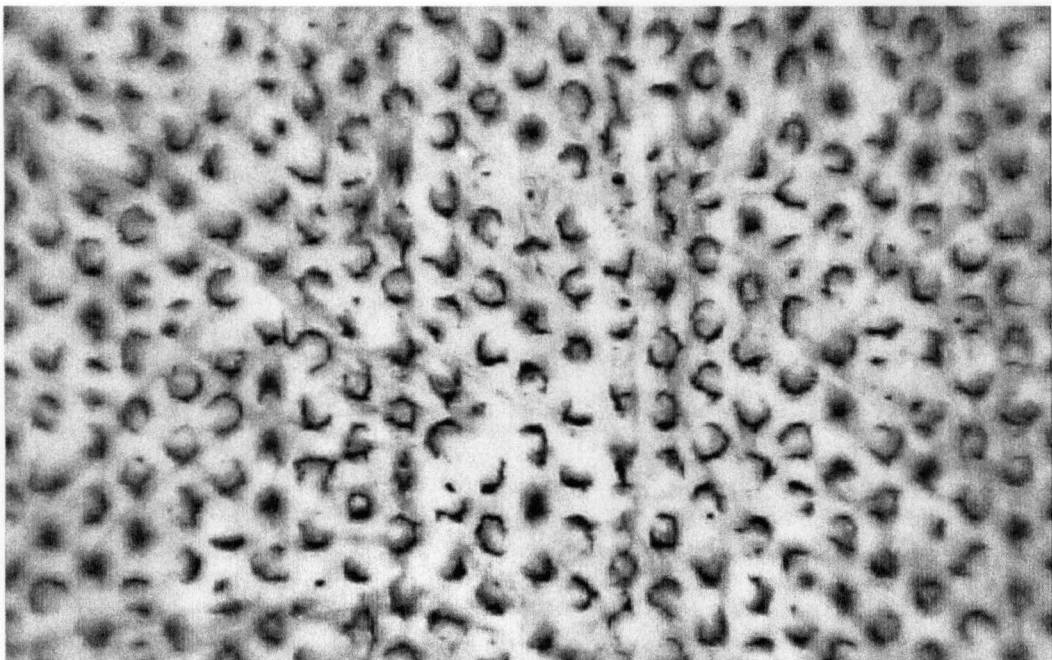Figure 46. Printing Image of 0T4N Coated Paper Printed With Water-Based Ink

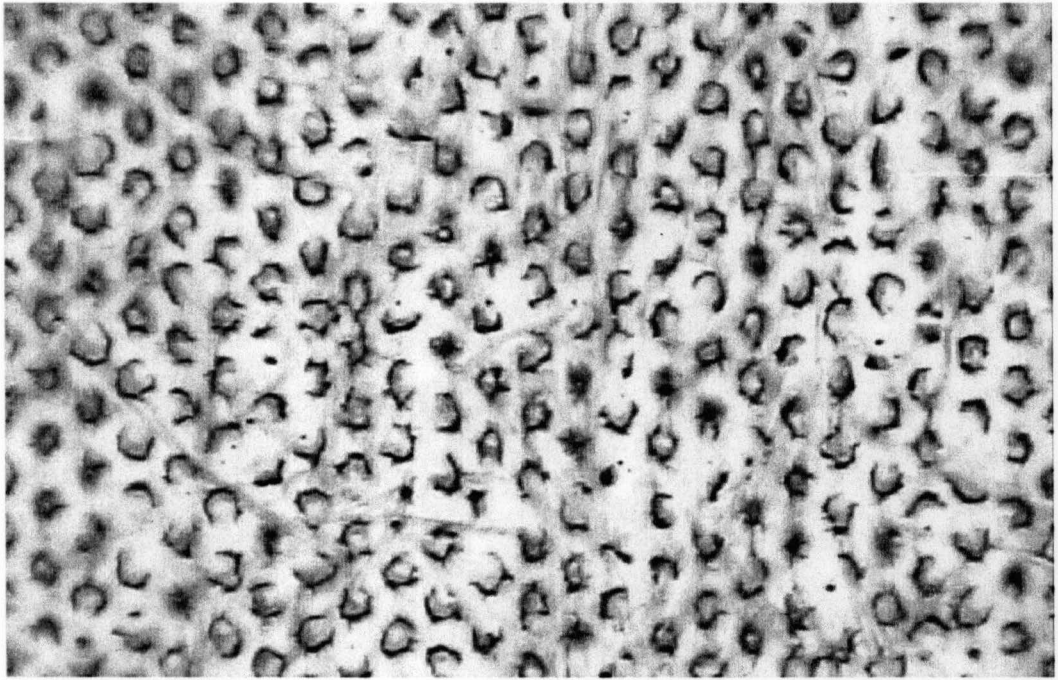Figure 47. Printing Image of 72D8S Coated Paper Printed With Water-Based Ink

Figure 48. Printing Image of 72D8N Coated Paper Printed With Water-Based Ink

LITERATURE CITED

1. Lepoutre, P., Skowronski, J., and Bichard, W., Tappi Coating Conference, Washington, p.113 (May 1986).

2. Skowronski, J., and Lepoutre, P., "Water Paper Interaction During Paper Coating", Tappi, J., 68(11): 98(1985).

3. Lehtinen, E., "Pigments Coatings and Surface Sizing of Papers," Finish Paper Engineers Assoc. and TAPPI Press, Atlanta, GA, p. 34-36, (2000).

4. Rooney, J. M., "Water-based Publication Gravure Inks" Sun Chemical Corporation, Convention Papers Gravure Week '89, 3rd Annual Convention of the Gravure Association of America, pp. 176-179 (March 1989).

5. Hmzewicz, N. J., Auerbach, R. and Sprycha, R., "Impact of Ink/Paper Interactions on Printability of Aqueous Publication Gravure Inks", Sun Chemical Corporation, p 38-46,Gravure / Winter (1998).

6. White, P. G., "Cylinder Requirements for Water-based Inks", Southern Graphic Systems, p 19, Gravure / Winter (1998).

7. Thompson, B., "Printing Materials: Science and Technology" PIRA, p. 329-330 (1998).

8. Lee, K. H., Joyce, M. K., Fleming, P. D., Cameron, J. H., "Production of a Single Coated Glossy Inkjet Paper Using Conventional Coating and Calendering Methods", Proceedings of the TAPPI Coating Conference, May 2002.

9. Lee, K. H., Joyce, M. K., Fleming, P. D., "Influence of Pigment Particle Size and Packing Volume on Printability of Glossy Inkjet Paper Coatings", Proceedings of the IS&T NIP19: International Conference on Digital Printing Technologies, New Orleans, October 2003.

10. Padigala, M., "Applications of Porous Media for Inkjet Coatings", Western Michigan University, 2002 MS Thesis Submitted

11. Ginman, R., "Paper Properties in Printing With Water-Based Gravure Inks", The Finish Pulp and Paper Research Institute, Helsinki, p 408-422 (1998).

12. Lepoutre, P., "Structure and performance of pigmented coatings: what do we know?" Proceedings of International Paper and Coating Chemistry Symposium, Ottawa, Canada, p.205 (1996).

13. Nisogi, H., Bousfield, D.W., and Lepoutre P.F., "Influence of Coating Rheology on Final Coating Properties", Tappi, J., 83(2): 100-105 (Feb 2000).

14. Bristow, J. A., Ekman, H., "Paper Properties Affecting Gravure Print Quality". Tappi 64(10): 115(Oct 1981).

15. Dunfield, L. G., McDonald, J. D., and Grattom, M. F., "Gravure Printability of Steam-Treated Machine Calendered Newsprint." Pulp and Paper J. 12(2): 31 (March 1986).

16. Ginman, R., "Paper Properties Required in Printing with Water-Based Gravure Inks." Advanced Printing Science Tech. 17 (Chap.26): 408-425 (June1983).

17. Qillett, K. E., "Gravure Process and Technology", GAA, Rochester, NY, pp. 5-58, 101-173, 241-329, 341-417 (1991).

18. Enright, D., "Water-Based Inks for Publication Gravure." Gravure, Fall/Winter, p. 30-32 (1993).

19. Serafano, J., and Triantafillopoulos, N., "Optimizing of ESA to Improve Ink Transfer" Ink World, p. 22-25, 67 (May 1993).

20. Siler, S. J., "Rediscover the color with ESA and Water-Based Inks" Gravure/ Winter, p. 52-55 (1999).

21. www.mineralgallery.com 2000, "The Zeolite Group of Minerals", Amethyst Gallery.

22. www.bza.org, "What is Zeolites, British Zeolite Association".

23. LaFaye, J. F., Maume, J. P., and Chiodi, R., "The Effect of Some Coating variables on Gravure Prints Quality Using Lightweight Coated Paper, Tappi J., p 63-69 (Dec 1988).

24. Lepoutre, P., "Substrate Absorbency and Coating Structure", Paper Coatings Tappi J., 61(5): 51(May 1978).

25. Arai, Y., Nojima, K., "Coating Structure for Obtaining High Print Gloss", Tappi J., 82(5): 213-221(1998).

26. Donigian, D. W., Ishley, J.W., and Wise, K.J., "Coating Pore Structure and Offset Print Gloss", Proceedings From the 1996 TAPPI Conference, p.39-48.

27. Lepoutre, P., Rigdahl, M., "Analysis of the Effect of Porosity and Pigment Shape on the Stiffness of Coating Layers", Journal of Material Science, 24(8)2971-2974 (1989).

28. Yamazaki, K., "Designing of Coating Color for Double Coating, Effect of Pigment and Binders in Under Coating", Japan Tappi, J., 53(6): 718-723 (1986).

29. Picollet, M., Piette, P., Morin, V. and LeNest, J.F., " Competition Between Gravure Ink Penetration and Spreading on LWC Coated Papers", Proceedings of the 1998 Tappi Coating / Papermakers Conference New Orleans, Tappi, Press, p 383-386.

30. Hiemenz, P.C., Rajagopalan, R., "Principles of Colloid and Surface Chemistry", NY p. 50, 265-286 (1997).

31. Adamson, A., and Gast, A. P., "Physical Chemistry of Surfaces", p. 5-35 (1997)

32. O'Boyle, R.C., "Water Based Inks for Packaging Films" Tappi, J., 74(8): 145-148 (Aug 1991).

33. Myers, D., "Surfaces, Interfaces, and Colloids", Principles and Applications, p. 349-379 (1988).

34. Michale, F.Y., Iwasa, S., Lavelle, T., Sunday, S., and Fetsko, T.M., "The Role of Wetting in Printing" TAGA, p309-329, (1989).

35. Bassemir, R.W., and Krishnan, R., "Practical Application of Surfaces Energy Measurements In Flexography." Sun Chemical Corporation, (1990).

36. Morra, M., Oaciello, E., Garbassi, F., "Knowledge about Polymer Surfaces from Contact Angle Measurement." Advances in Colloid and Interface Science, p. 33, 79-116 (1990).

37. Lepoutre, P., DeGrace, J.H., Mangin, J.P., "Influence of Coating Absorbency On The Printability of Coated papers" Proceedings From the 1979 Tappi Coating Conference, OH, p.21-23.

38. Zang, Y.H., Aspler, J.S., "The influence of Coating Structure on the Ink Rceptivity and Print Gloss Development of Model Clay coatings". International Printing and Graphic Arts Conference, p. 193-199 (1994).

39. www.galleries.com/minerals/silicates/zeolites, "The Zeolite Group of Minerals".

40. Londo et al., "Coating Pigment for Ink-Jet Printing", United States Patent-5997625, Engelhard Corporation, Iselin, N.J., Dec. 7, 1999.

41. Christopher, W. M., "Rheology Principles, Measurements, and Applications", NY p. 337-373 (1993).

42. Triantafillopoulos, G. N., "Paper Coating Viscoelasticity And its Significance in Blade Coating", TAPPI Press, Atlanta, GA, p. 11-22 (1996).

43. Abrams, L., Favorite, C., Capano, P., and Johnson, R., "Using Mercury Porosimetry to Characterize Coating Pore Structure and Its Relation to Optical Properties", TAPPI Coating Conference Proceedings, Atlanta, p. 185 (1996).

44. Sarafano, J., and Pekarovicova, A., "Factors Affecting Dot Fidelity in Solvent Based Publication Gravure." American Ink Maker, p. 77, 32-36 (1999).